Structure and Infrastructure Engineering

Maintenance, Management, Life-Cycle Design and Performance

ISSN: (Print) (Online) Journal homepage: https://www.tandfonline.com/loi/nsie20

Methodology to account for the impact of stress history in layered soils for seismic vulnerability assessment of scoured bridges

Yijian Zhang & Iris Tien

STRUCTURE AND INFRASTRUCTURE ENGINEERING
https://doi.org/10.1080/15732479.2020.1860096

Taylor & Francis
Taylor & Francis Group

Methodology to account for the impact of stress history in layered soils for seismic vulnerability assessment of scoured bridges

Yijian Zhang and Iris Tien

School of Civil and Environmental Engineering, Georgia Institute of Technology, Atlanta, GA, USA

ABSTRACT
Scour has been recognized as one of the leading causes of bridge collapse in the United States. Therefore, it is essential to be able to build models that accurately capture the response of bridges vulnerable to scour, including those located in layered rather than homogeneous soil deposits. Simple removal of soil springs due to scour ignores the effect of stress history for layered soils, which can lead to unconservative designs of foundations. This article proposes a methodology called the equivalent stress history and layered effects (ESHaLE) approach to capture the impact of soil stress history of layered soils on vulnerability assessment of scoured bridges. It utilises conservation of strength and mass to derive corresponding soil and depth parameters. Results show that neglecting to include stress history impacts in layered soils can lead to an underestimation of the single pile axial displacements by up to 35% in static analysis, and underestimation of the probability of exceeding bridge deck deflection thresholds by up to 25% in seismic fragility assessment. The study presents a method to include both soil stress history and layered effects in soil modeling and shows the importance of including these soil effects in the assessment of bridges vulnerable to scour.

ARTICLE HISTORY
Received 26 April 2020
Accepted 19 October 2020

KEYWORDS
Bridges; fragility assessment; layered soils; numerical method; scour; seismic analyses; soil stress history; soil–structure interaction

1. Introduction

Due to the erosive action of flowing water, material is carried away from the bed and banks of a stream, often leading to scour conditions for water-crossing bridge structures. The loss of soils surrounding the bridge foundation can lead to the loss of load-carrying capacity of the foundation system. Previous studies have shown that scour at bridge foundations is a major cause of bridge collapse (Wardhana & Hadipriono, 2003), with 60% of bridge failures in the U.S. related to vulnerabilities caused by scour (Lagasse, Clopper, Zevenbergen, & Girard, 2007). With the importance of scour on the predicted performance of bridges, it is essential to be able build models that accurately capture the response of scoured bridges.

In the past decade, researchers have studied the seismic performance of bridges in the presence of scour (Alipour, Shafei, & Shinozuka, 2013; Banerjee & Ganesh Prasad, 2013; Fioklou & Alipour, 2019; Wang, Dueñas-Osorio, & Padgett, 2014). However, these studies employ traditional modeling of scour with simple removal of soil springs without considering the changes of stress states and corresponding properties of the remaining soil due to scour. Meanwhile, other studies have investigated the influence of soil stress history on laterally loaded single piles in sand and soft clay (Lin, Bennett, Han, & Parsons, 2010; Lin, Han, Bennett, & Parsons, 2014). These studies show that neglecting the stress history effect can lead to unconservative responses of scoured piles. However, most of the previous studies regarding the effect of stress history still focus on a homogeneous soil type. At the same time, it is common for bridges to be located at sites with layered soil deposits (Aygun, 2009; Soneji & Jangid, 2008; Takemiya & Yamada, 1981). Modeling profiles consisting of layers of multiple soil types as a homogeneous material neglects the layered soil effects. Researchers have investigated the lateral (Davisson & Gill, 1963; Gazetas & Dobry, 1984; Georgiadis, 1983; Zhang, Zhao, & Zou, 2015) and the vertical (Cairo & Conte, 2006; Huang, Liang, & Jiang, 2011; Wang, Xie, & Wang, 2012) behaviors of piles in layered soil deposits. However, these studies do not account for the impact of stress history in layered soils, and most do not focus on addressing vulnerability assessment of full bridge structures. In summary, there have been no previous studies on the effect of soil stress history on the properties of layered soils. In addition, evaluating the seismic performance of bridges subject to scour including the effect of soil stress history of layered soils is unstudied. This article proposes a methodology to account for the influence of both layered deposits and soil stress history in evaluating the performance of bridges susceptible to scour. The method includes the ability to analyse profiles that consist of both sandy and clayey soils. This article is the first to account for the stress history effects for layered soils, with the main contributions being presentation of the new equivalent stress history and layered effects (ESHaLE) approach and results showing the importance of taking such an approach in the vulnerability assessment of scoured bridges. Using the proposed methodology enables

CONTACT Yijian Zhang zyj.albert@gatech.edu School of Civil and Environmental Engineering, Georgia Institute of Technology, Atlanta, GA, USA

the vulnerability of bridges located in layered soil deposits that are susceptible to scour to be more accurately and comprehensively assessed.

The rest of the article is structured as follows. The next section introduces background information regarding first, the effect of soil stress history for a single homogeneous soil deposit and second, the behavior of layered soils due to multiple heterogeneous deposits. The following section describes in detail the proposed ESHaLE methodology for combining the effects of soil stress history and layered soils for the modeling and analysis of bridges susceptible to scour. The next section applies the methodology to an example bridge and soil profile. Results from using ESHaLE compared to unmodified soil models in the vulnerability assessment of a scoured bridge under seismic loading are shown. Finally, concluding remarks and a summary of findings are provided.

2. Background and related work

2.1. Stress history of soils

The deposition of soils can be viewed as a loading process, while scour can be viewed as an unloading process as surrounding soils are removed. Due to the unloading process, the remaining soil after scour experiences different stress states, leading to changes in the soil properties. In particular, the soils change from normally consolidated to overconsolidated states (Brown & Castelli, 2010), represented by an overconsolidation ratio (OCR) between the previous maximum stress and present stress. The OCR increases as scour depth increases, leading to changes in the soil properties. Detailed information regarding calculating the changes in the soil properties due to the effect of stress history in sandy (Lin et al., 2010) and clayey (Lin et al., 2014) soils is provided in the Appendix.

Soils are traditionally modeled using springs in three directions: *p-y* springs model lateral soil behavior, *t-z* springs model vertical soil behavior including the skin friction between the pile and soil, and q-z springs model behavior at the pile tip. For cohesionless soils (e.g. sand), including the effect of soil stress history due to scour reduces the relative density, unit weight, and modulus of subgrade reaction, and increases the friction angle and OCR of the remaining soil (Lin et al., 2010). Reese, Cox, and Koop (1974) propose a *p-y* relation for sand, with the ultimate resistance for wedge failure near the ground surface (P_{st}) and flow failure well below the ground surface (P_{sd}) computed based on Equations (1) and (2), respectively.

$$P_{\mathrm{st}} = \gamma' z\left\{\frac{K_o z\ \tan(\phi')\sin(\beta)}{\tan(\beta-\phi')\cos(\alpha)} + \frac{\tan(\beta)}{\tan(\beta-\phi')}\left[B + z\tan(\beta)\tan(\alpha)\right] + K_o z\ \tan(\beta)\left[\tan(\phi')\sin(\beta) - \tan(\alpha)\right] - K_a B\right\} \tag{1}$$

$$P_{\mathrm{sd}} = K_a B\gamma' z\left[\tan^8(\beta) - 1\right] + K_o B\gamma' z\ \tan(\phi')\tan^4(\beta) \tag{2}$$

γ' is effective unit weight of sand, z is distance between mudline and point of interest, β is passive failure angle, α is angle defining the shape of the failure wedge, K_a is minimum coefficient of active earth pressure, K_o is coefficient of lateral earth pressure at rest, B is diameter of the pile, and ϕ' is friction angle.

This study adopts the *p-y* relation shown in Equation (3) for sand from the American Petroleum Institute (API, 2000) in combination with Equations (1) and (2) to compute the ultimate lateral resistance of sand. $P_{\mathrm{ult}_{\mathrm{sand}}}$ in Equation (3) is computed based on the minimum value between P_{st} and P_{sd} depending on the depth of interest obtained from Equations (1) and (2), respectively.

$$P = AP_{ult_{sand}}\tanh\left[\frac{kH}{AP_{ult_{sand}}}y\right] \tag{3}$$

P is lateral soil resistance at any depth H, A is a modification factor that accounts for static or cyclic loading (0.9 in this case), P_{ult} is ultimate bearing capacity at depth H, y is lateral deflection, and k is initial modulus of subgrade reaction.

The effect of the soil stress history is accounted for by updating the relative density and coefficient of lateral earth pressure of the remaining sand after scour due to the change from normally consolidated to overconsolidated soil. The change of relative density is caused by the changes of the void ratio and overburden stress, which leads to the change of additional properties of sand, including unit weight, modulus of subgrade reaction, and friction angle.

For *t-z* relations, the ultimate unit shaft resistance of sand ($T_{ult_{sand}}$) is computed as in Equation (4) (Touma & Reese, 1974), where $\sigma_v{}'$ is effective vertical stress at a point of interest.

$$T_{ult_{sand}} = 0.7\tan(\phi')\sigma_v{}' \tag{4}$$

The ultimate end bearing resistance ($Q_{ult_{sand}}$) of sand is computed based on Mayerhof (1976) with Equation (5).

$$Q_{ult_{sand}} = N_q\sigma_v{}' \tag{5}$$

N_q is a dimensionless bearing capacity factor. The *t-z* relation for sand is adopted based on Mosher (1984), which uses a hyperbolic representation of the *t-z* curve as shown in Equation (6).

$$T = \frac{z}{\frac{1}{E_f} + \frac{1}{T_{ult_{sand}}}(z)} \tag{6}$$

E_f is the value of the initial modulus, z is movement of pile segment, and T is total shear transfer. The backbone of the *q-z* curve for sand is approximated using Vijayvergiya's relation (1977) shown in Equation (7).

$$Q = \left(\frac{z}{z_c}\right)^{\frac{1}{3}} * Q_{ult_{sand}}\ \ (z \le z_c) \tag{7a}$$

$$Q = Q_{ult_{sand}}\ \ (z > z_c) \tag{7b}$$

Q is pile tip resistance and z_c is movement required to mobilise $Q_{ult_{sand}}$ (6.35 mm for sand).

The change of remaining properties of sand due to stress history can also affect the vertical behavior of sand (i.e. $T_{ult_{sand}}$ and $Q_{ult_{sand}}$), and these changes are also considered in this study. More details regarding capturing stress history of sand can be found in Lin et al. (2010).

For cohesive soils (e.g. soft clay), the ultimate soil resistance ($P_{ult_{sand}}$) is computed as in Equation (8) (Matlock, 1970).

$$P_{ult_{clay}} = \min\left\{\left(3 + \frac{\gamma'}{C_u}z + \frac{J}{B}z\right)C_uB, 9C_uB\right\} \tag{8}$$

C_u is undrained shear strength of clay and J is set as a constant with a value of 0.5. The p-y relation for soft clay is adopted from Matlock (1970). $P_{ult_{clay}}$ of stiff clay without free water can also be computed based on Equation (8) (Reese & Welch, 1975; Welch & Reese, 1972). Stiff clay without free water indicates a stiff clay layer located above the water table. As the OCR and scour depth change, including the soil stress history also influences the effective unit weight and undrained shear strength of soft clay. While the change of the effective unit weight is insignificant, the undrained shear strength has been found to be significantly reduced when the effect of soil stress history is considered (Lin et al., 2014). The ultimate unit shaft resistance of clay is computed according to Equation (9) (Tomlison, 1992).

$$T_{ult_{clay}} = \alpha C_u \tag{9}$$

α is an adhesion factor for piles in clay, which can be computed by Equation (10).

$$\alpha = 0.5\psi^{-0.5}(\psi \leq 1.0) \tag{10a}$$

$$\alpha = 0.5\psi^{-0.25}(\psi > 1.0) \tag{10a}$$

ψ is the ratio between undrained shear strength of the soil (C_u) and effective overburden pressure (σ_v') at the point of interest. Note that the value of α should not exceed 1.0. The t-z relation for clay is adopted from Reese and O'Neill (1987). The computation of point-bearing capacity ($Q_{ult_{clay}}$) of clay is based on Terzaghi's bearing capacity theory (Terzaghi, 1943). Due to the characteristics of cohesive soils and piles, the relation can be simplified to Equation (11), where A_p is cross-sectional area of the pile.

$$Q_{ult_{clay}} = 9A_pC_u \tag{11}$$

The q-z relation for clay is adopted based on Reese and O'Neill (1987). The change of the vertical response of clay accounting for soil stress history effects is also considered in this study, manifested through the decrease in undrained shear strength (C_u). The change in undrained shear strength after scour is quantified and established based on critical state soil mechanics and expressed as a function of the OCR (Lin et al., 2014).

2.2. Behavior of layered soils

To account for the behavior of layered soils, previous studies have calculated 'equivalent' soil depths, for example, using conservation of strength to obtain the p-y behavior for layered soil deposits (Georgiadis, 1983).

As p-y curves only apply to homogeneous soil deposits, the p-y curve for a profile with successive layers of different soil types is determined using a series of equivalent depth calculations. For example, the equivalent depth of a second soil layer is found by first calculating the force (F_1) acting at the layer interface as shown in Equation (12).

$$F_1 = \int_0^{D_1} P_{\text{ult}1}\,dH \tag{12}$$

$P_{\text{ult}1}$ is the ultimate soil resistance of the first layer and D_1 is the thickness of the first layer. The equivalent depth ($X_{\text{py}2}$) of the first soil layer that includes the characteristics of the soil deposit from the second layer is then obtained by solving Equation (13).

$$F_1 = \int_0^{X_{\text{py}2}} P_{\text{ult}2}\,dH \tag{13}$$

$P_{\text{ult}2}$ is the ultimate soil resistance of the second layer.

The same procedure is applied to obtain the equivalent depth for the second layer including the soil deposit of the third layer, and so on through the layers in the soil profile. This approach has been verified experimentally (Georgiadis, Anagnostopoulos, & Naskos, 1999) for a single pile loaded laterally and vertically in layered soils. The effect of layered soils in the vertical direction is considered for both sands and clays through evaluating the value of effective vertical stress. The theoretical basis is that the effective vertical stress is a function of effective unit weight, which changes from layer to layer, and composite action is required to maintain the continuity of strength in the vertical direction. For sands, the ultimate axial resistances of sand ($T_{ult_{sand}}$ and $Q_{ult_{sand}}$) are a function of vertical effective stress as indicated in Equations (4) and (5). For clays, the ultimate unit shaft resistance ($T_{ult_{clay}}$), as shown in Equation (9), is a function of both undrained shear strength (C_u) and alpha (α), where the value of alpha is a function of effective vertical stress (σ_v'). Meanwhile, the ultimate end bearing resistance ($Q_{ult_{clay}}$) of clay is assumed to be only a function of undrained shear strength (C_u) as shown in Equation (11).

In this article, the authors take an equivalent depth approach to model behavior of layered soils. However, in addition to conservation of strength, conservation of mass is utilised to account for the effect of soil stress history in layered soils. The proposed approach is described in detail in the following section.

3. Proposed equivalent stress history and layered effects methodology (ESHaLE)

3.1. Equivalent depth based on conservation of mass

The process of scour removes soils, unloading and reducing the effective vertical stress acting on the remaining soil. Figure 1 shows the consolidation curve of clay under scour conditions considering the soil stress history. The subscripts int and sc represent parameters before and after scour, respectively. σ_v' is effective vertical stress, e is void ratio of soil, C_c is compression index, and C_r is recompression index. The soil stress history leads to a change in vertical effective stress, which leads to a change in void ratio.

Sand will exhibit similar consolidation behavior except for changing the value on the x-axis from σ_v' to the mean effective stress P', where P' is used to quantify the change

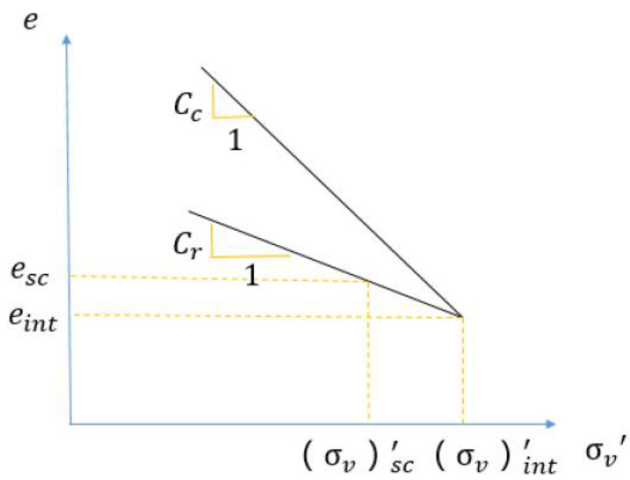

Figure 1. Consolidation curve of clay under scour conditions.

of effective pressure. P' can be also represented in terms of effective vertical stress as shown in Equation (14), where $\sigma_h{}'$ is effective horizontal stress.

$$P' = \frac{\sigma'_v + 2\sigma'_h}{3} \tag{14a}$$

$$P' = \left(\frac{1 + 2K_o}{3}\right)\sigma'_v \tag{14b}$$

The objective is to find an equivalent scour depth and equivalent layer depths that account for the changes in the soil parameters due to stress history effects. The change in effective vertical stress is obtained based on conservation of mass as follows. Consider first a soil profile with two layers. The stress history effect in the lower layer is accounted for with the partial or full removal of the upper layer. The change in effective vertical stress is quantified by the mass loss due to the removal of the soil as if it only consists of soil material from the lower layer. This holds for general scour conditions, which neglects the effect of scour hole dimensions in the case of local scour conditions. An 'equivalent' scour depth is then found, which is computed based on conservation of mass.

In general, for a layered soil deposit with layer i and $i+1$ as shown in Figure 2, let D_i be the depth of layer i and S_d the scour depth. z_{pi} is the distance between the initial mudline and point of interest, and z_{sc} the distance between the new mudline after scour and point of interest. Each point of interest corresponds with a soil spring for which the parameters must be updated. The objective is to find an equivalent depth of layer i in terms of the layer $i+1$ soil material, (D_{i_e}), an equivalent scour depth (S_{d_e}), and equivalent distances z_{sc_e} and z_{pi_e}.

The equivalent scour depth and layer depth for a layer i are calculated based on conservation of mass as shown in Equations (15a) and (15b), using the ratio of effective unit weights between adjacent layers. Next, z_{sc_e} and z_{pi_e} are computed based on the geometric relations shown in Figure 2 combined with the relations shown in Equations (15a) and (15b). The expressions for the equivalent distances are derived in terms of effective unit weights, scour depth, and layer depth, as shown in Equations (15c) and (15d).

$$S_{d_e} = \frac{\gamma'_i}{\gamma'_{i+1}} S_d \tag{15a}$$

$$D_{i_e} = \frac{\gamma'_i}{\gamma'_{i+1}} D_i \tag{15b}$$

$$z_{sc_e} = z_{sc} + \left(\frac{\gamma'_i}{\gamma'_{i+1}} - 1\right)(D_i - S_d) \tag{15c}$$

$$z_{pi_e} = z_{sc_e} + S_{d_e} \tag{15d}$$

γ'_i is effective unit weight of layer i and γ'_{i+1} is effective unit weight of layer $i+1$. Once the equivalent depths and distances are found, the values of S_{d_e} and z_{sc_e} can be used to compute the updated soil properties including the effect of soil stress history as if the soil consists of a homogeneous layer with the detailed procedures presented in the Appendix (Figures A1 and A2). Note that the Equation (15) is only applicable for the scenario indicated in Figure 2 where the point of interest is located within the second layer and scour occurs within the first layer. To generalise to other scenarios, new expressions for S_{d_e} and z_{sc_e} need to be determined. The following sections present a comprehensive set of these expressions for soils with two and three layers and with varying scour depths. With this proposed methodology, the effect of stress history can be accounted for in any soil layers of interest.

3.2. Overall approach to account for stress history effects in layered soils

The goal is to obtain modified p-y, t-z, and q-z relations given scour depth and the soil profile considering both the stress history and layered soil effects. The stress history effect is applied to the soil model first to obtain updated soil properties after scour. Next, the equivalent depths due to the layered effect are calculated based on the updated properties of the soil layer. This sequence is chosen such that the equivalent depth can be calculated based on the most up-to-date soil properties, including the stress history effects, enabling more realistic and accurate results. Finally, the p-y, t-z, and q-z parameters (i.e. ultimate soil resistance) are determined based on the combined updated soil properties and equivalent depths. Figure 3 shows the overall procedure of the proposed methodology.

3.3. Parameters for soils with multiple layers

To accurately model the soil springs after scour including the effect of soil stress history for layered soils, the soil parameters at varying points of interest below the mudline must be calculated. Each point of interest, an example of which shown in Figure 2, corresponds with the location of a specific soil spring. The derived expressions for the parameters for different points of interest below the mudline are now provided. The first case considered is a soil deposit with two layers. Figure 4 shows the four scenarios for this case, with varying scour depths S_d and locations of points of interest below the mudline. D_i is the initial soil layer depth, z_{pi} the distance between the initial mudline and point of

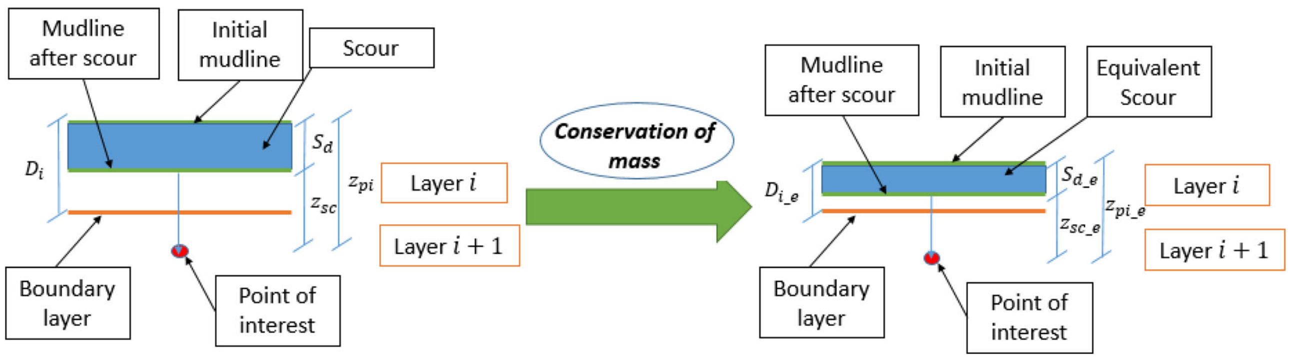

Figure 2. Finding equivalent layer depth and scour depth for layered soils accounting for stress history effects based on conservation of mass.

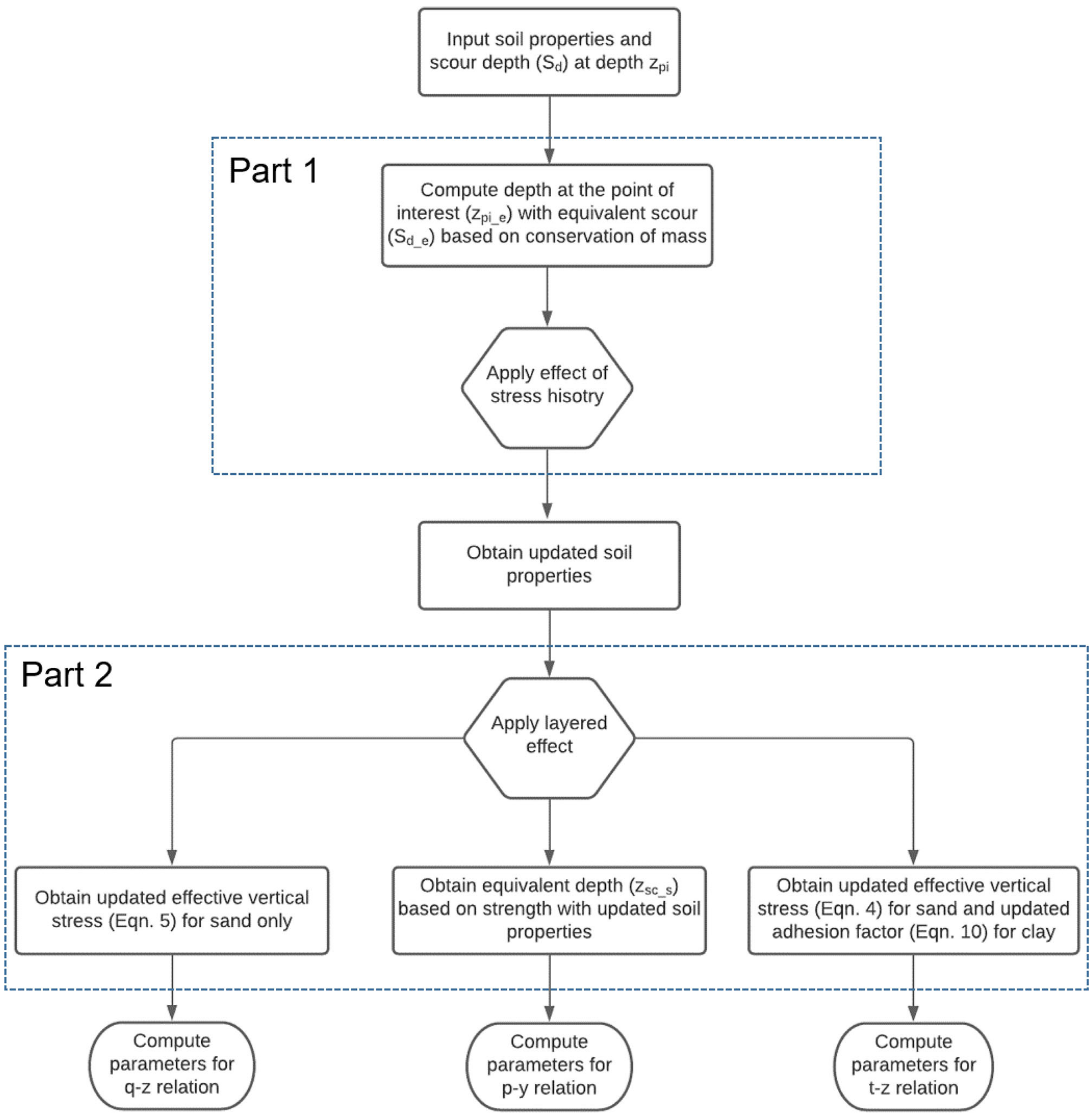

Figure 3. Proposed approach to account for soil stress history and layered effects in layered soil profiles.

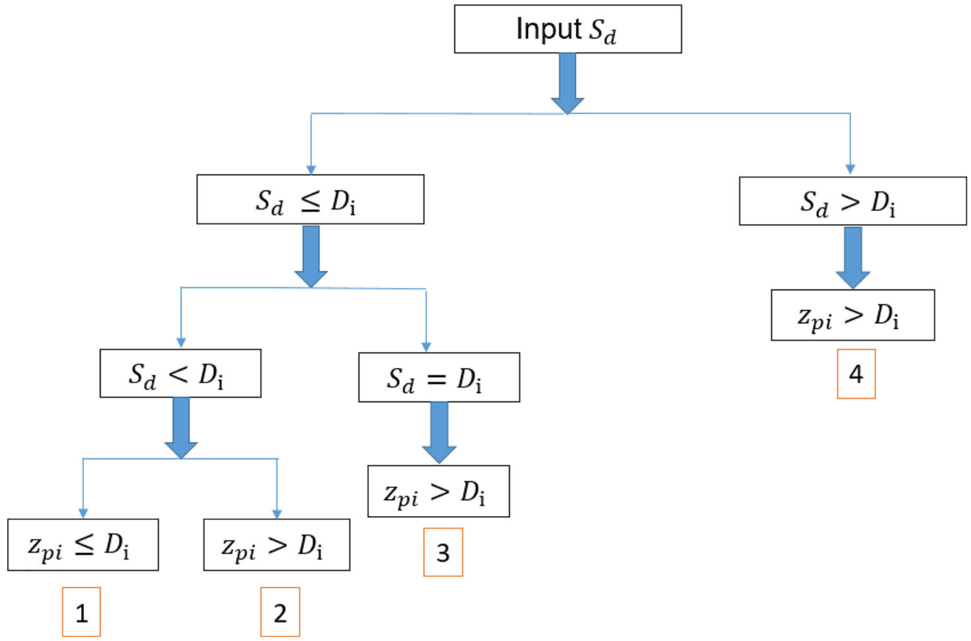

Figure 4. Four scenarios for varying scour depths and points of interest below the mudline for two-layered soil deposits.

Table 1. Equivalent quantities for soil deposits with two layers.

Scenario	S_{d_e}	z_{sc_e}	z_{sc_s}	X_{pyk}
1	S_d	z_{sc}	z_{sc}	–
2	$\frac{\gamma_i'}{\gamma_{i+1}'} S_d$	$z_{sc} + \left(\frac{\gamma_i'}{\gamma_{i+1}'} - 1\right)(D_i - S_d)$	$z_{sc} + X_{py2} + S_d - D_i$	$\int_0^{D_i - S_d} P_{ult_{py_i}} dH = \int_0^{X_{py2}} P_{ult_{py_{i+1}}} dH$
3	$\frac{\gamma_i'}{\gamma_{i+1}'} S_d$	z_{sc}	z_{sc}	–
4	$\left(\frac{\gamma_i'}{\gamma_{i+1}'} - 1\right) D_i + S_d$	z_{sc}	z_{sc}	–

interest, and z_{sc} the distance between the new mudline after scour and point of interest.

For each scenario shown in Figure 4, modified values of S_d and z_{sc} need to be computed to account for the combined soil stress history and layered soil effects. The symbolic expression for each term as derived based on the proposed methodology is shown in Table 1. Two equivalent depths are calculated: z_{sc_e} is the equivalent value calculated based on conservation of mass, which is used to determine the updated soil properties due to the effect of soil stress history; and z_{sc_s} is the equivalent value calculated based on conservation of strength, which is used to determine the ultimate soil resistance. In the calculation of z_{sc_s}, an additional term X_{pyk} is needed. X_{pyk} is a value of equivalent depth that accounts for the layered effect in the lateral direction, with the subscript k representing the term for the kth scenario. The value of X_{pyk} is computed by numerical integration of the equation shown in the rightmost column of Table 1. $P_{ult_{py_i}}$ is the ultimate soil resistance of layer i in the lateral direction.

The next case considered is a soil deposit with three layers. Instead of four separate scenarios as for a two-layered deposit, there are now a total of nine scenarios. Figure 5 shows a point of interest among layers $i-1$, i, and $i+1$, where the scour occurs only partially in layer $i-1$. D_{i-1} is the depth of layer $i-1$. The scenario where the scour extends into the second layer is also addressed in the table of derived equivalent quantities given in Table 2. Figure 6 shows the nine scenarios corresponding to the varying scour depths and points of interest for three-layered soil deposits. The equivalent quantities derived for each of the nine scenarios shown in Figure 6 are given in Table 2.

For soil deposits with more than three layers, the number of scenarios will further increase, but a similar methodology can be applied to derive the equivalent quantities. The derived expressions presented in Tables 1 and 2 and the analysis procedure shown in Figure 3 comprise the proposed ESHaLE approach.

4. Example soil profile and single pile test

4.1. Details of selected soil profile

An example soil profile is chosen from the literature (Aygun, 2009) to illustrate the results of implementing the proposed methodology. To obtain a realistic soil profile for bridge foundations, fifty blueprints of existing bridges in South Carolina were analysed (Aygun, 2009). The profile chosen for this study is shown in Figure 7 and is typical of low lands stratigraphy. The soil profile consists of three

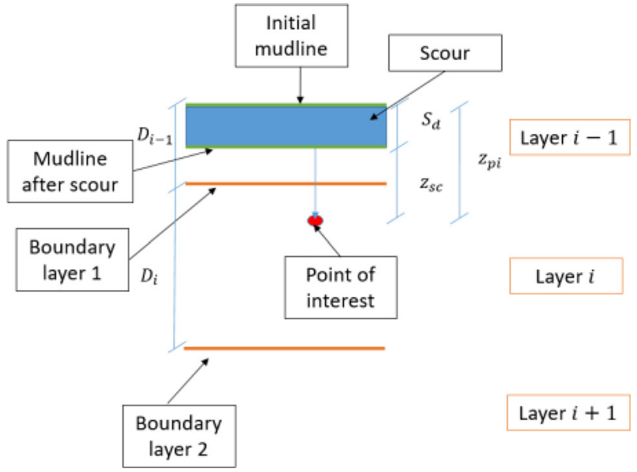

Figure 5. Scoured soil deposit with three layers and point of interest below the mudline.

layers with the properties of each layer specified based on typical soil conditions (Yang, Lu, & Elgamal, 2008). The concrete pile for the bridge is assumed to be 18 m in length with a 2 m circular diameter, which is also shown in Figure 7.

For this soil profile, the results from three models are shown to compare the outcomes from varying modeling approaches to evaluate the ultimate resistance of soil. The first model represents the basic approach with simple removal of soil springs due to scour without any modification. This model is referred to as 'UMD' in the rest of this article, representing an *unmodified* soil model. The second model includes only the effect of layered soils, modeled using equivalent depth calculations. This model is referred to as 'LEO' in the rest of this article, representing a model that accounts for the *layered effect only*. The third model is the proposed *ESHaLE* model that includes both the soil

Table 2. Equivalent quantities for soil deposits with three layers.

Scenario	S_{d_e}	z_{sc_e}	z_{sc_s}	X_{pyk}
1	S_d	z_{sc}	z_{sc}	–
2	$\frac{\gamma'_{i-1}}{\gamma'_i} S_d$	$z_{sc} + \left(\frac{\gamma'_{i-1}}{\gamma'_i} - 1\right)(D_{i-1} - S_d)$	$z_{sc} + X_{py2} + S_d - D_{i-1}$	$\int_0^{D_{i-1}-S_d} P_{\mathrm{ult}_p y_{i-1}} dH = \int_0^{X_{py2}} P_{\mathrm{ult}_p y_i} dH$
3	$\frac{\gamma'_{i-1}}{\gamma'_{i+1}} S_d$	$z_{sc} + \left(\frac{\gamma'_{i-1}}{\gamma'_{i+1}} - 1\right)(D_{i-1} - S_d) + \left(\frac{\gamma'_i}{\gamma'_{i+1}} - 1\right) D_i$	$z_{sc} + X_{py3} + S_d - D_{i-1} - D_i$	$\int_0^{D_i+X_{py2}} P_{\mathrm{ult}_p y_i} dH = \int_0^{X_{py3}} P_{\mathrm{ult}_p y_{i+1}} dH$
4	$\frac{\gamma'_{i-1}}{\gamma'_i} S_d$	z_{sc}	z_{sc}	–
5	$\frac{\gamma'_{i-1}}{\gamma'_{i+1}} S_d$	$z_{sc} + \left(\frac{\gamma'_i}{\gamma'_{i+1}} - 1\right) D_i$	$z_{sc} + X_{py5} + S_d - D_i$	$\int_0^{D_i} P_{\mathrm{ult}_p y_i} dH = \int_0^{X_{py5}} P_{\mathrm{ult}_p y_{i+1}} dH$
6	$\left(\frac{\gamma'_{i-1}}{\gamma'_i} - 1\right) D_{i-1} + S_d$	z_{sc}	z_{sc}	–
7	$\left(\frac{\gamma'_{i-1}}{\gamma'_{i+1}} - \frac{\gamma'_i}{\gamma'_{i+1}}\right) D_{i-1} + \frac{\gamma'_i}{\gamma'_{i+1}} S_d$	$z_{sc} + \left(\frac{\gamma'_i}{\gamma'_{i+1}} - 1\right)(D_{i-1} + D_i - S_d)$	$z_{sc} + X_{py7} + S_d - D_{i-1} - D_i$	$\int_0^{D_{i-1}+D_i-S_d} P_{\mathrm{ult}_p y_i} dH = \int_0^{X_{py7}} P_{\mathrm{ult}_p y_{i+1}} dH$
8	$\frac{\gamma'_{i-1}}{\gamma'_{i+1}} D_{i-1} + \frac{\gamma'_i}{\gamma'_{i+1}} D_i$	z_{sc}	z_{sc}	–
9	$\left(\frac{\gamma'_{i-1}}{\gamma'_{i+1}} - 1\right) D_{i-1} + \left(\frac{\gamma'_i}{\gamma'_{i+1}} - 1\right) D_i + S_d$	z_{sc}	z_{sc}	–

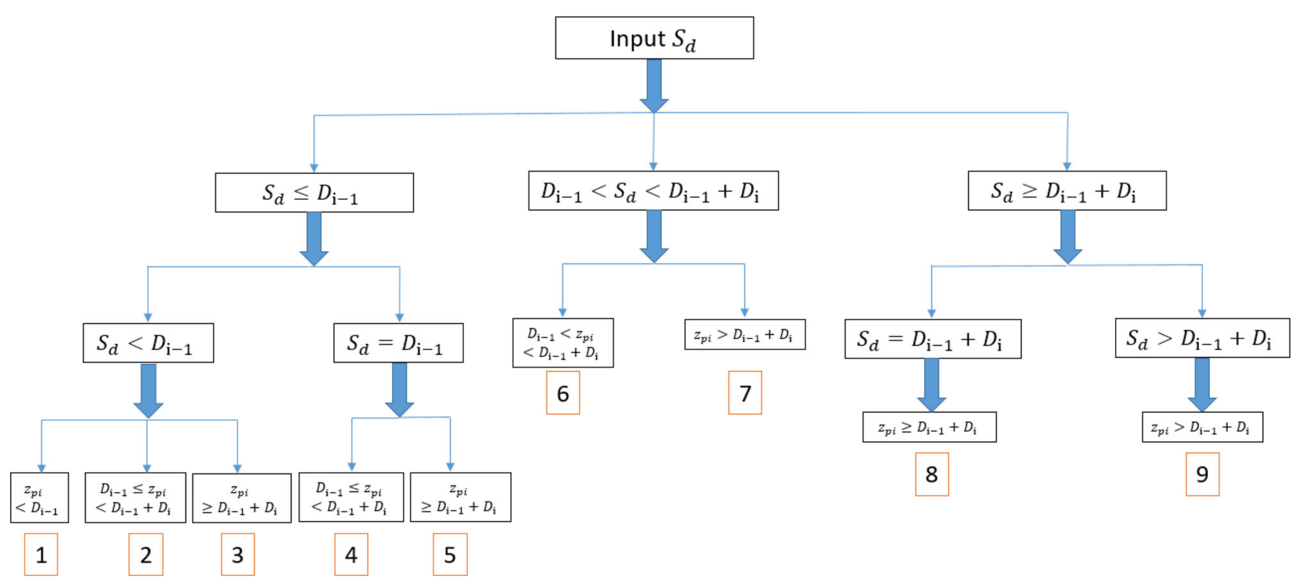

Figure 6. Nine scenarios for varying scour depths and points of interest below the mudline for three-layered soil deposits.

stress history and layered soil effects. The comparison is conducted first between the UMD and ESHaLE models, and next between the LEO and ESHaLE models.

Figure 8 shows the resulting ultimate lateral resistance of soil, comparing the UMD and ESHaLE models, in 1 m intervals along the depth of the pile and for scour depths (S_d) ranging from 1 m to 9 m. Although 9 m of scour is large relative to the structural dimensions, it is included for illustrative purposes to account for the extreme condition and the scenario such that the first two soil layers have been removed due to scour. At each scour depth, the solid line indicates the result from using the ESHaLE model; the dashed line indicates the result using the UMD model. Figure 8(a) compares the values of the ultimate lateral resistance of soil (P_{ult}) along the length of the pile as soil depth increases from the UMD and ESHaLE models. Figure 8(b) shows the percentage difference between the two models. The two boundary layers in the profile are also indicated.

In Figure 8, the UMD resistance curve is the same across scour depths except for the first point for each level of scour because in the unmodified model, an increase in scour depth does not affect the soil behavior. The varying initial points are because the resistance of the first point is assumed to be half of the next point. For the initial point, when scour depth is 1 m, the difference between the

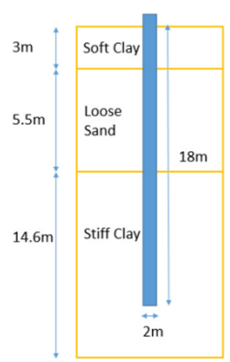

Figure 7. Representative soil profile and pile geometry.

ESHaLE and UMD models is relatively small. However, as scour depth increases, the maximum percentage difference increases significantly, up to 2000% in the sand layer for a scour depth of 7 m.

Figure 9 shows the comparison of ultimate unit shaft resistance (T_{ult}) between the UMD and proposed ESHaLE models. Similar to the lateral behavior shown in Figure 8, the ultimate unit shaft resistance using the UMD model follows the same line regardless of the scour level except for the first point. At the first point, the differences between using the UMD and ESHaLE models can still be significant, with a maximum reduction of up to 700% in ultimate unit shaft resistance, occurring in the sand layer with 7 m scour depth. In Figure 9, the ESHaLE model results in smaller soil resistance values along the depth of pile for all scour levels. This is because accounting for the layered soil effect in the proposed approach results in smaller equivalent depths compared with the physical depths used in the UMD model.

The unmodified (UMD) model is usually adopted in practice, accounting the effect of scour by simply removing the soil springs in the scoured area without considering any additional effects. Alternative existing models account for the layered effect only (LEO). A comparison between the LEO model and proposed ESHaLE model – which accounts for stress history in addition to layered soil effects – has also been conducted. Figure 10(a) compares the calculated ultimate lateral resistance of soil (P_{ult}) along the depth of the pile that is obtained from using the LEO (dashed line) and proposed ESHaLE (solid line) models as scour depth increases. Figure 10(b) gives the percentage difference between the two models.

Several interesting points can be observed from Figure 10. First, there is a reduction of ultimate resistance for both LEO and ESHaLE models at the second interface for 1 m and 3 m scour depths, which is due to the layered effect from the first two layers. Second, when the scour depth is larger than 3 m, the stress history effect dominates. This is observed because the soil stress history of clay reduces its

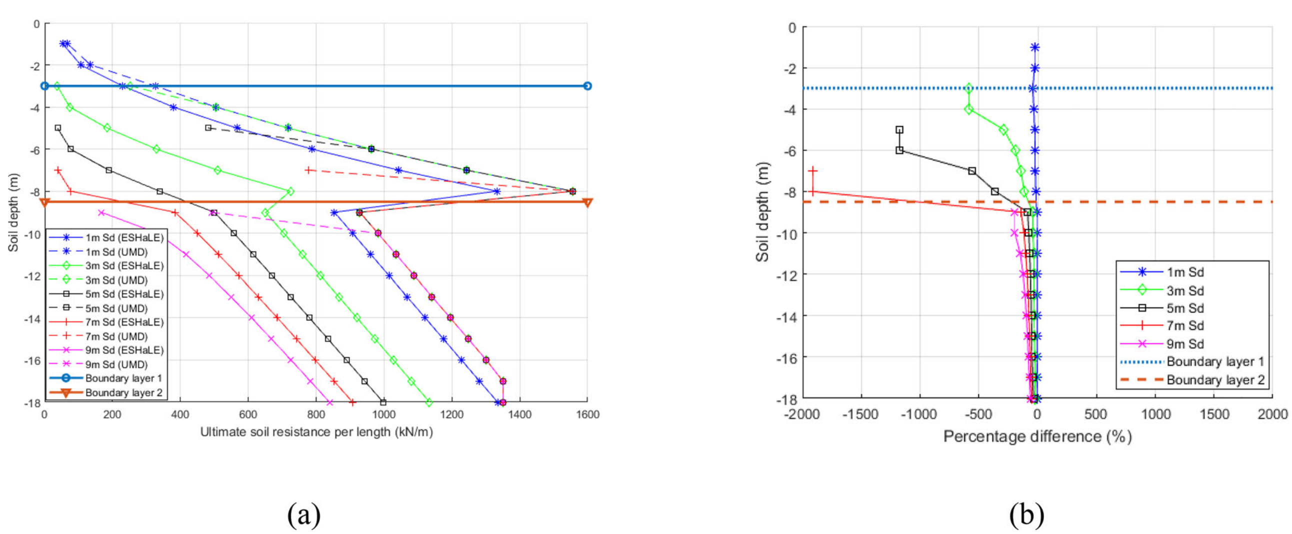

Figure 8. (a) Comparison of ultimate lateral resistance (P_{ult}) between proposed ESHaLE and UMD models at varying scour depths and (b) percentage difference between the two models.

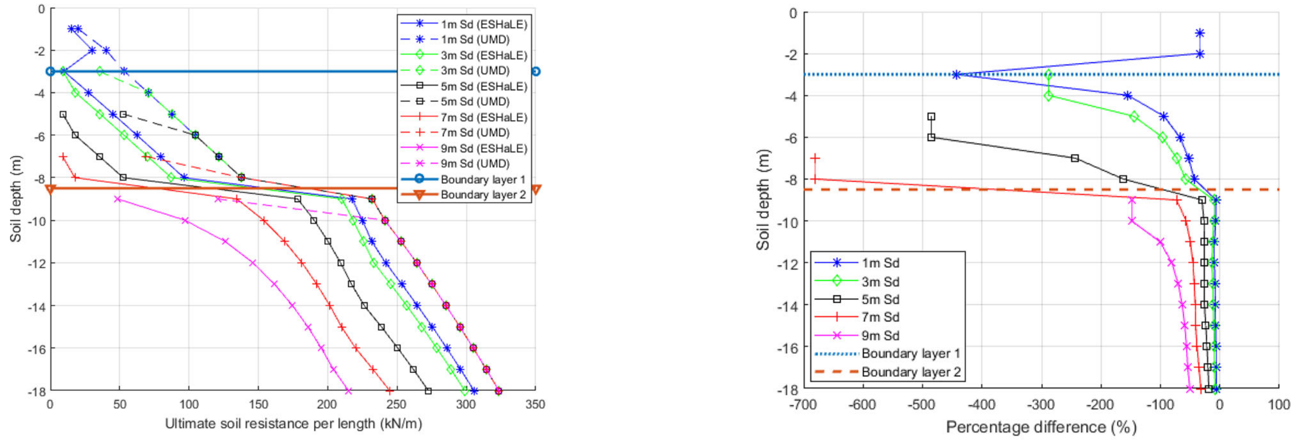

(a) (b)

Figure 9. (a) Comparison of ultimate vertical resistance (T_{ult}) between proposed ESHaLE and UMD models at varying scour depths and (b) percentage difference between the two models.

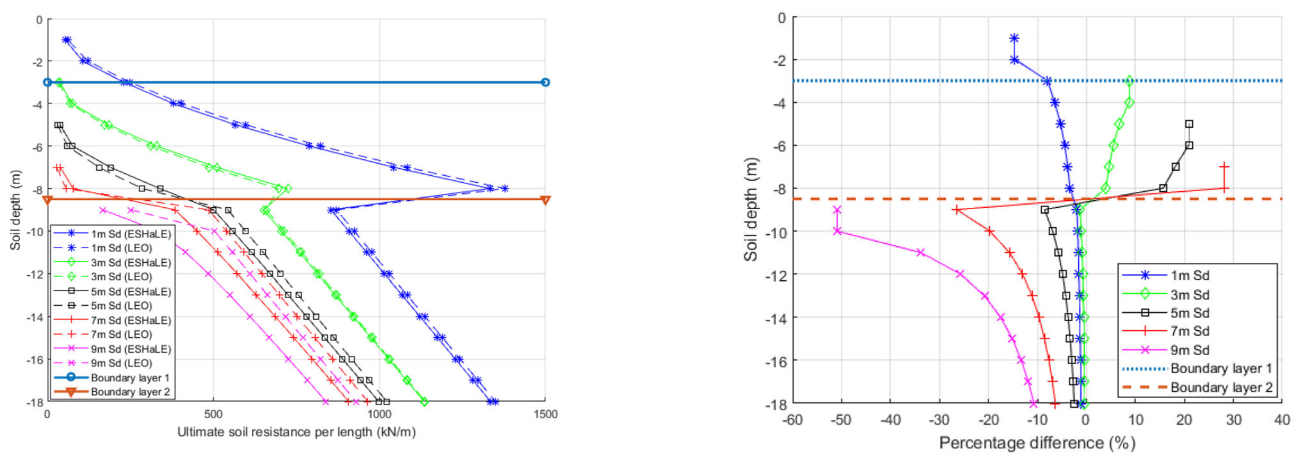

(a) (b)

Figure 10. (a) Comparison of ultimate lateral resistance (P_{ult}) between proposed ESHaLE and LEO models at varying scour depths and (b) percentage difference between the two models.

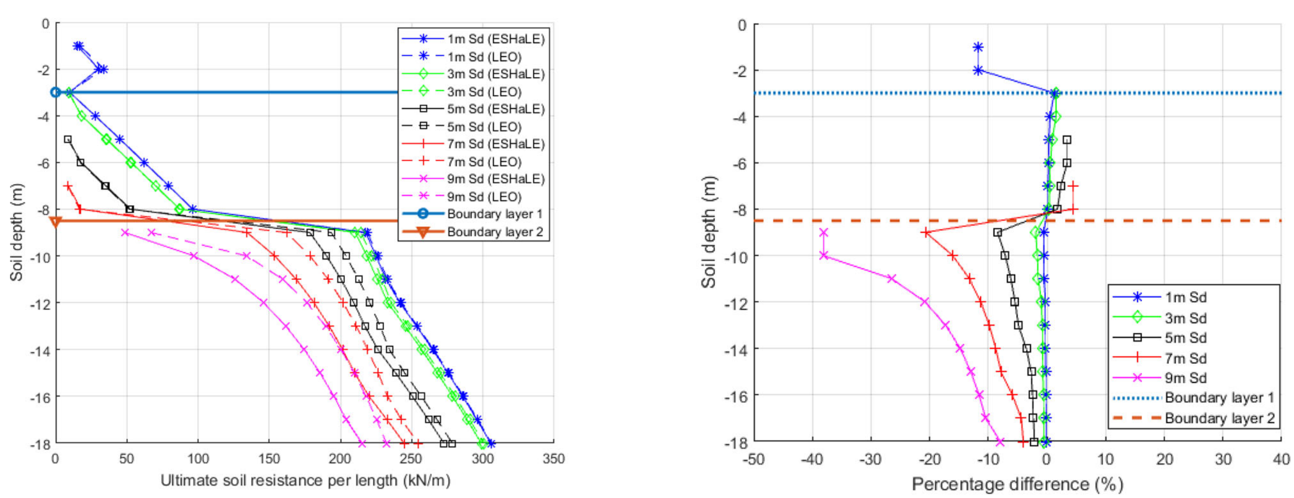

(a) (b)

Figure 11. (a) Comparison of ultimate vertical resistance (T_{ult}) between proposed ESHaLE and LEO models at varying scour depths and (b) percentage difference between the two models.

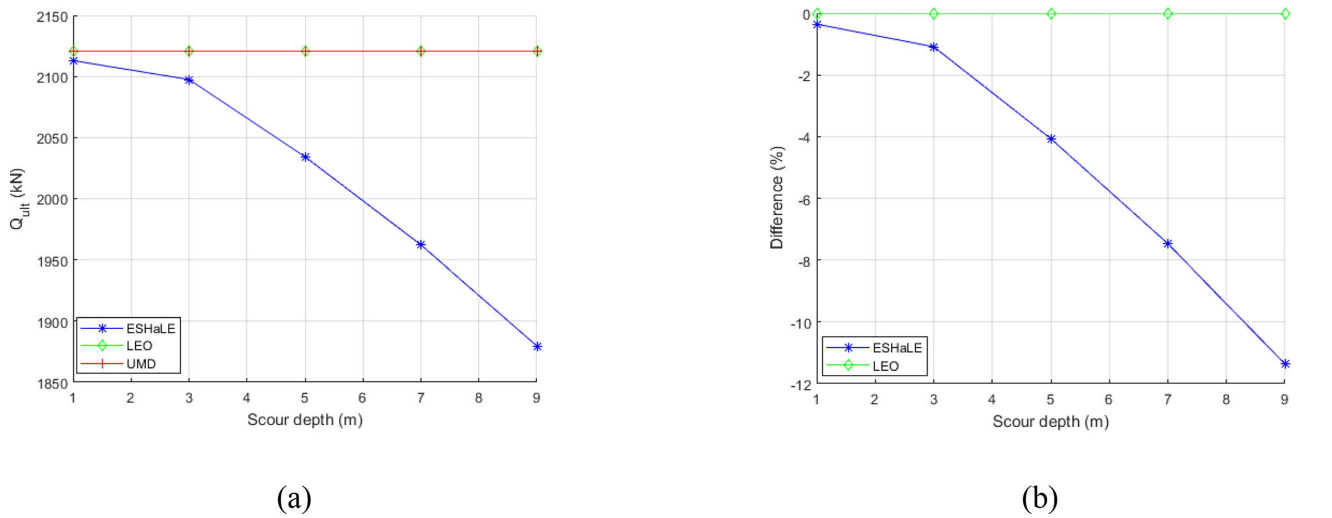

Figure 12. (a) Comparison of ultimate bearing resistance (Q_{ult}) between proposed ESHaLE, LEO, and UMD models at varying scour depths and (b) percentage difference between the three models.

ultimate lateral resistance while the stress history of sand increases its resistance. In comparison, when the scour depth is less than 3 m, the layered effect is more pronounced, as is observed from the result from the third layer. Third, the importance of accounting for the stress history effect and not only the layered effect is observed, with a maximum percentage difference in the soil ultimate lateral resistance between the LEO and ESHaLE models of around 50%.

Figure 11 shows the ultimate unit shaft resistance of soil (T_{ult}) between the LEO and ESHaLE models. Figure 11(a) shows that the stress history effect reduces the vertical resistance of clay because the unloading process associated with scour reduces the value of the undrained shear strength, which is proportional to T_{ult} of clay. In comparison, the stress history effect increases the vertical resistance of sand because both friction angle and unit weight increase in the presence of scour. Moreover, there is a reduction at the first boundary for both models, due to loose sand yielding a smaller ultimate lateral resistance even after accounting for the contribution to the strength of the first layer. Figure 11(b) shows the importance of accounting for stress history effects in addition to layered soil effects, as the maximum percentage difference between the LEO and ESHaLE models is close to 38%, occurring in the clay layer with a scour depth of 9 m.

Figure 12(a) presents a comparison among all three models in terms of ultimate bearing capacity (Q_{ult}) at varying scour depths. Figure 12(b) shows the percentage difference between the ESHaLE and LEO models and the results from a baseline UMD model. For this soil profile, the bearing resistance is provided by stiff clay only. Figure 12 shows the UMD and LEO models give a constant bearing resistance regardless of scour level. In comparison, the ESHaLE model results in a decreased calculated bearing resistance as scour depth increases. This is because the stress history effect reduces the undrained shear strength of the clay. The next section presents results regarding a single pile test with lateral and vertical loadings applied separately at the top of the pile considering the ESHaLE, LEO, and UMD soil models.

4.2. Verification and single pile test

Verification of the proposed method with numerical and experimental results is now provided. An extensive review of the literature has shown that experimental data regarding scour effects on the structural performance of piles is scarce. At the same time, numerical models that capture the impact of stress history in layered soils under scour conditions are also lacking in the literature. Therefore, the authors verify the proposed ESHaLE framework by parts, as indicated in Figure 3. Part 1 verifies the effect of stress history in homogeneous soils under scour using both experimental tests and numerical models. Part 2 verifies the layered effect using experimental results. Details regarding the verification of each part are now shown.

Comparing results from the ESHaLE model with results from experimental tests and numerical models in homogeneous soils considering scour provides verification of the stress history effects captured in ESHaLE. As only a homogeneous soil is presented, $S_d = S_{d_e}$ and $z_{pi} = z_{pi_e}$, verifying the accuracy of the ESHaLE model within only an individual soil layer, but considering both stress history and scour effects. Verification is provided for both sand and soft clay. For the analysis in a sand foundation, for an initial condition, results from ESHaLE are compared with experimental field pile tests without scour as a baseline. Table 3 shows the soil properties for the uniformly graded fine sand from Mustang Island, Texas (Cox, Reese, & Grubbs, 1974). As shown in Figure 13(a), the laterally loaded pile has a length, outer diameter, and thickness of 21.3 m, 0.61 m, and 0.0095 m, respectively. The effect of scour is analysed by comparing results from the ESHaLE model with those from a numerical model obtained using LPILE Plus 5.0 from Lin et al. (2010) considering a scour depth of 3 m as well as the effect of stress history. The ESHaLE model is implemented in the finite element platform OpenSees (McKenna, 1997). Figure 13(b) presents the results for verification. Compared with the pre-scoured condition, 3 m scour depth increases the pile lateral deflection at the ground line due to the removal of soil. The results from the ESHaLE model and numerical model from Lin et al. (2010) are close, with the

Table 3. Properties of sand (Cox et al., 1974).

Critical friction angle (°)	Effective unit weight (kN/m^3)	Relative density (%)	Maximum void ratio	Minimum void ratio	Specific gravity
28.5	10.4	70 (depth $\leq$ 3 m)90 (depth $\geq$ 3 m)	1.0	0.598	2.65

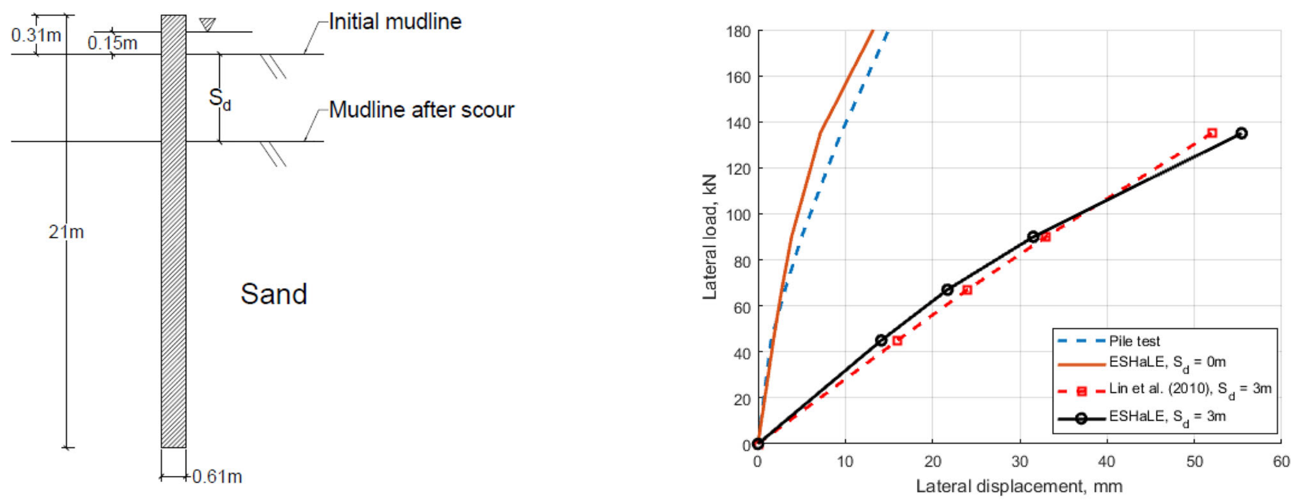

(a) (b)

Figure 13. (a) Laterally loaded pile in uniform fine sand and (b) deflection at ground line versus laterally applied load for measured data and numerical models with the effect of stress history under scour.

Table 4. Properties of soft clay.

Effective unit weight (kN/m^3)	Water content (%)	Compression index	Swelling index	Strain at half of maximum stress	Effective friction angel (°)
10	44.5	0.38	0.076	0.012	20

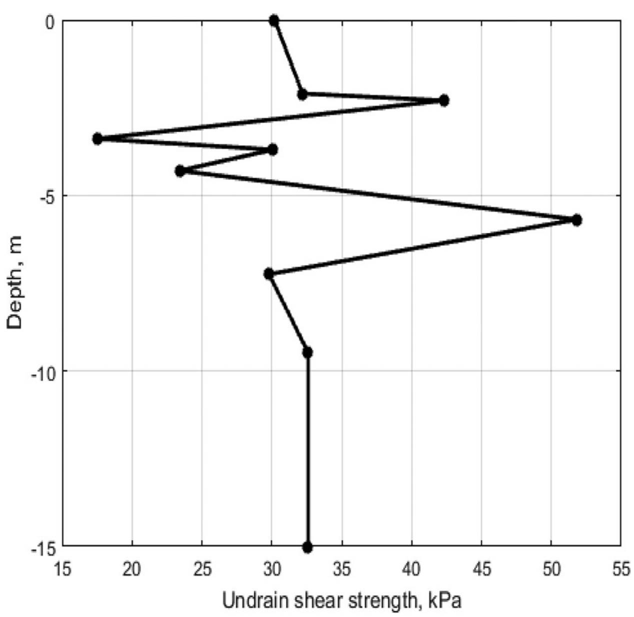

Figure 14. Distribution of undrained shear strength of soft clay measured by Reese and Van Impe (2001).

discrepancy mainly due to the different selection of *p-y* relations between the two models. Lin et al. (2010) adopt the *p-y* relation from Reese et al. (1974), whereas the current study uses the *p-y* relation from API shown in Equation (3) available in OpenSees. The resulting difference between the two models is small with an average difference of 8.0%.

Next, a similar verification process is performed for a single pile embedded in a clay foundation. The soil is soft clay near Lake Austin, Texas, with pile test conducted by Matlock (1970) for baseline pre-scour conditions. The soil properties are listed in Table 4, and the undrained shear strength along the depth of the soil is shown in Figure 14 (Reese & Van Impe, 2001). Figure 15(a) shows the geometry of the laterally loaded pile in clay. Figure 15(b) shows the of pile-head deflection versus laterally applied load for ESHaLE results compared with both experimental and numerical results. The numerical result from Lin et al. (2014) is obtained using LPILE 5.0 considering the effect of stress history and scour. The value of scour depth (S_d) used for comparison is 10*B*, where *B* is the diameter of the pile. The difference between the results from ESHaLE and the numerical model from Lin et al. (2014) is small due to the use of the same *p-y* relation (Matlock, 1970) and methodology to account to the effect of stress history, with an average difference of 2.3%.

The first part of the verification verifies the ability of ESHaLE to capture scour and stress history effects. The second part of the verification focuses on the ability of the proposed approach to capture layered soil effects. Results from the ESHaLE model are compared with results from experimental tests for a single pile loaded laterally and vertically in layered soils under no scour conditions ($S_d = 0$) as shown in Figure 16(a) (Georgiadis et al., 1999). Note that the LEO model is equivalent to ESHaLE model when

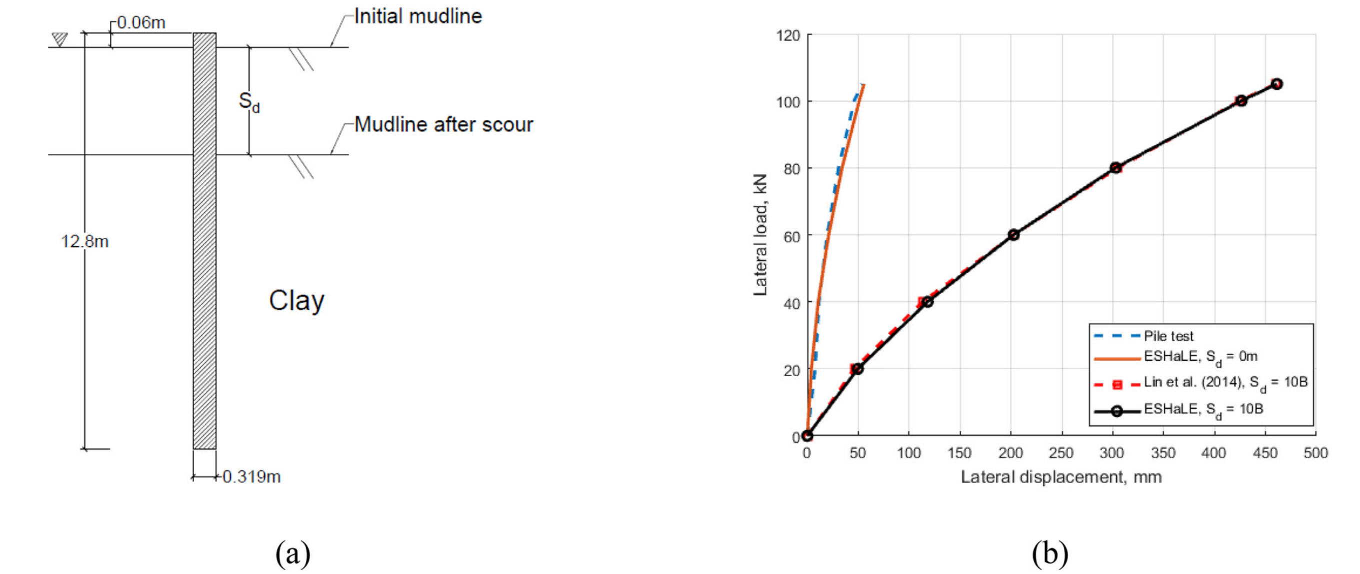

Figure 15. (a) Laterally loaded pile in soft clay and (b) pile-head deflection versus laterally applied load for measured data and numerical models with the effect of stress history under scour.

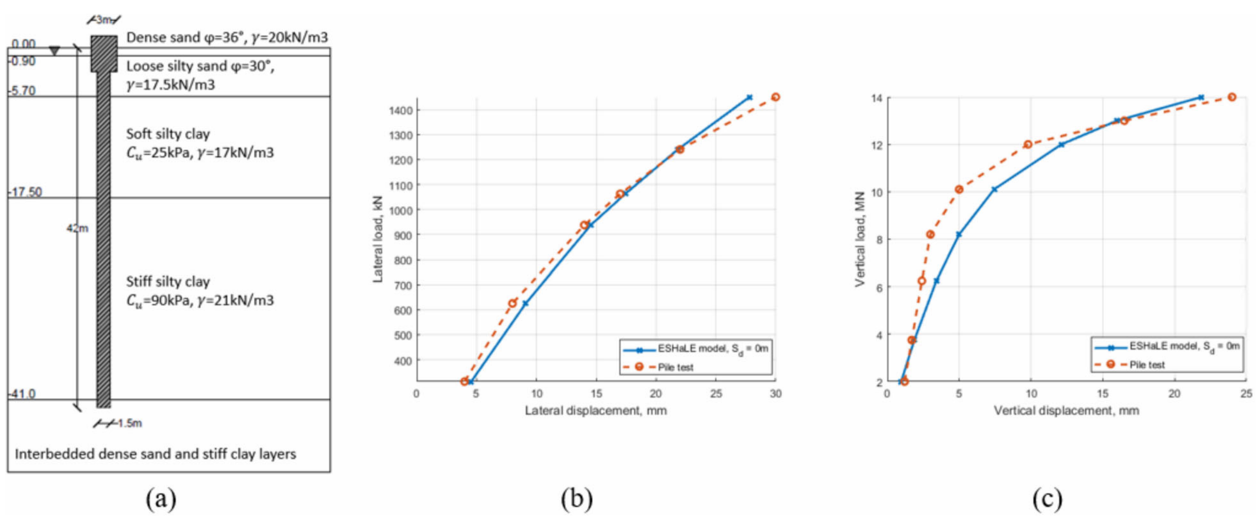

Figure 16. (a) Setup of pile test and soil profile (Georgiadis et al., 1999), (b) lateral load versus pile head lateral displacement, and (c) axial load versus pile settlement for ESHaLE model compared with experimental pile test in layered soil.

considering responses in layered soils with no scour. Further verification between the ESHaLE and LEO models is conducted for single pile test results that follow. For the experimental test, the full scale pile has a total length of 42.0 m with 3 m diameter from ground level to a depth of 3.0 m and 1.5 m below this depth. The pile test is subjected to an axial load and subsequently to a lateral load using hydraulic jacks. The soil profile is derived from a geotechnical site investigation. Figure 16 shows the details regarding the pile geometry, design soil profile, and verification of the ESHaLE model with experimental results in terms of the lateral and vertical displacements versus applied loads. The results shows close agreement between the results from the ESHaLE model and those from the pile test, especially in the lateral direction, where the displacement differences range from 0.2 mm to 2.2 mm, with an average percent difference of 7.1%. For the vertical direction, the larger difference between the numerical and experimental results, with displacement differences ranging from 0.2 mm to 2.4 mm and an average percent difference of 27.1%, is mainly due to the lack of information regarding the modeling of the *q-z* behavior of the bottom soil layer. The bottom layer consists of interbedded dense sand and stiff clay and the finite element platform OpenSees only allows modeling of *q-z* relations with homogenous soil types, while the authors have found that the ultimate end-bearing capacity as well as the choice of *q-z* relation used at the base of the pile to simulate soil-structure interaction will impact the overall results. Note that the verification results in this section are comparable to the verification of previous numerical models with experimental test results, where, for example, in Georgiadis et al. (1999), displacement differences range from 0.0 mm to 3.0 mm with an average percent difference of 6.0% for lateral loads, and displacement differences range from 0.0 mm to 7.5 mm with an average percent difference of 19.9% for vertical loads.

The proposed ESHaLE model is now implemented and compared to prior models through investigating the lateral

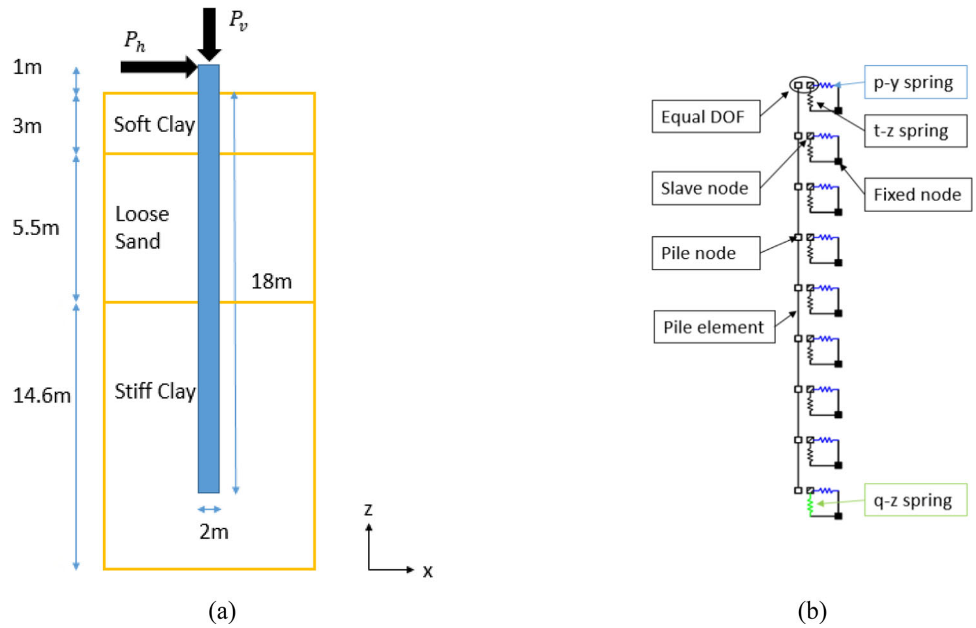

Figure 17. (a) Schematics of single pile and (b) modeling of the soil-structure interaction with lateral and vertical loadings applied separately in layered soil.

and vertical responses from the ESHaLE, LEO, and UMD models for a single pile test in the soil profile shown in Figure 7. Note that the results from the proposed ESHaLE model would be identical to those from the LEO model under conditions of zero scour. The results shown in this section also serve to explore the structural performance across scour depths of a laterally and vertically loaded pile in layered soil considering the different soil models under static loading. Figure 17(a) presents the geometry, applied loads, and composition of the layered soil used in this example. The pile has a diameter of 2 m, embedded length of 18 m, and pile head length of 1 m, and it is modeled as a beam on a nonlinear Winkler foundation using OpenSees. The pile consists of 19 displacement-based beam-column elements with discretised length of 1 m between nodes, and the constitutive material is assumed to be linear elastic for simplicity. Figure 17(b) shows the modeling of the soil-structure interaction. The soil springs, which consist of *p-y*, *t-z*, and *q-z* springs, are modeled using zero-length elements with uniaxial material assigned in lateral and vertical directions separately. This analysis considers applying a lateral load (P_h) of 1000 kN and a vertical load (P_v) of 2000 kN in the positive x direction and negative *z* direction, respectively.

Figure 18(a) shows results for the displacement along the pile under a laterally applied load (P_h) with varying scour depths of 0 m, 1 m, and 3 m. The main observations are as follows. First, the lateral responses from the ESHaLE and LEO models converge at 0 m scour depth as no scour event has occurred. A minimal difference between the ESHaLE and LEO models is observed at 1 m scour depth, which indicates the impact of stress history on the lateral behavior of piles is limited for small scour depths in terms of pile deflection. As scour level increases, the difference between the ESHaLE and LEO increases, indicating the effect of stress history on the response. Second, the UMD soil model gives unreliable deflection results due to the fact that the UMD model assumes no change has been made to soil parameters (i.e. P_{ult}, T_{ult}, and Q_{ult}) in the presence of scour and neglects the influence of the layered soil effect. The difference, i.e. error, between the UMD and other two models increases as the scour level increases. Figure 18(b,c) present the corresponding shear and moment diagrams along the pile in response to the laterally applied load.

To examine the vertical performance of the pile considering varying scour depths and different soil models, Figure 19(a) shows the maximum axial displacement of the pile after applying a vertical load of 2000 kN at the pile head considering varying scour depths. Consistent with previous soil responses, the pile with the ESHaLE model exhibits the highest axial displacement with a maximum increase of more than 110% at a scour depth of 9 m in comparison with the response from the UMD model as shown in Figure 19(b). Unlike the response from the laterally loaded pile, the impact of stress history is significant in terms of the axial response, with a maximum increase of 30% between the ESHaLE and LEO models at a scour depth of 9 m. The difference is mainly attributed to the reduction of end-bearing capacity with the inclusion of the effect of stress history in ESHaLE as shown in Figure 12. In both Figures 15 and 16, as expected, at minimum scour depths, the difference between the ESHaLE and previously verified LEO model is minimal. Finally, while results are shown here for single pile foundations, the ESHaLE model will also work for pile groups with the note that the ESHaLE model is only valid under the assumption of a general scour scenario. For cases where the effects of local scour are of interest, the scour hole geometry will impact single piles and pile groups differently. Future research can incorporate the ESHaLE model together with the influence of scour hole geometry in layered soils for both single piles and pile groups.

The next section shows how the differences in calculated soil properties (i.e. the varying ultimate soil resistance values shown in this section) from using the ESHaLE compared to layered effect only and unmodified soil models impact the

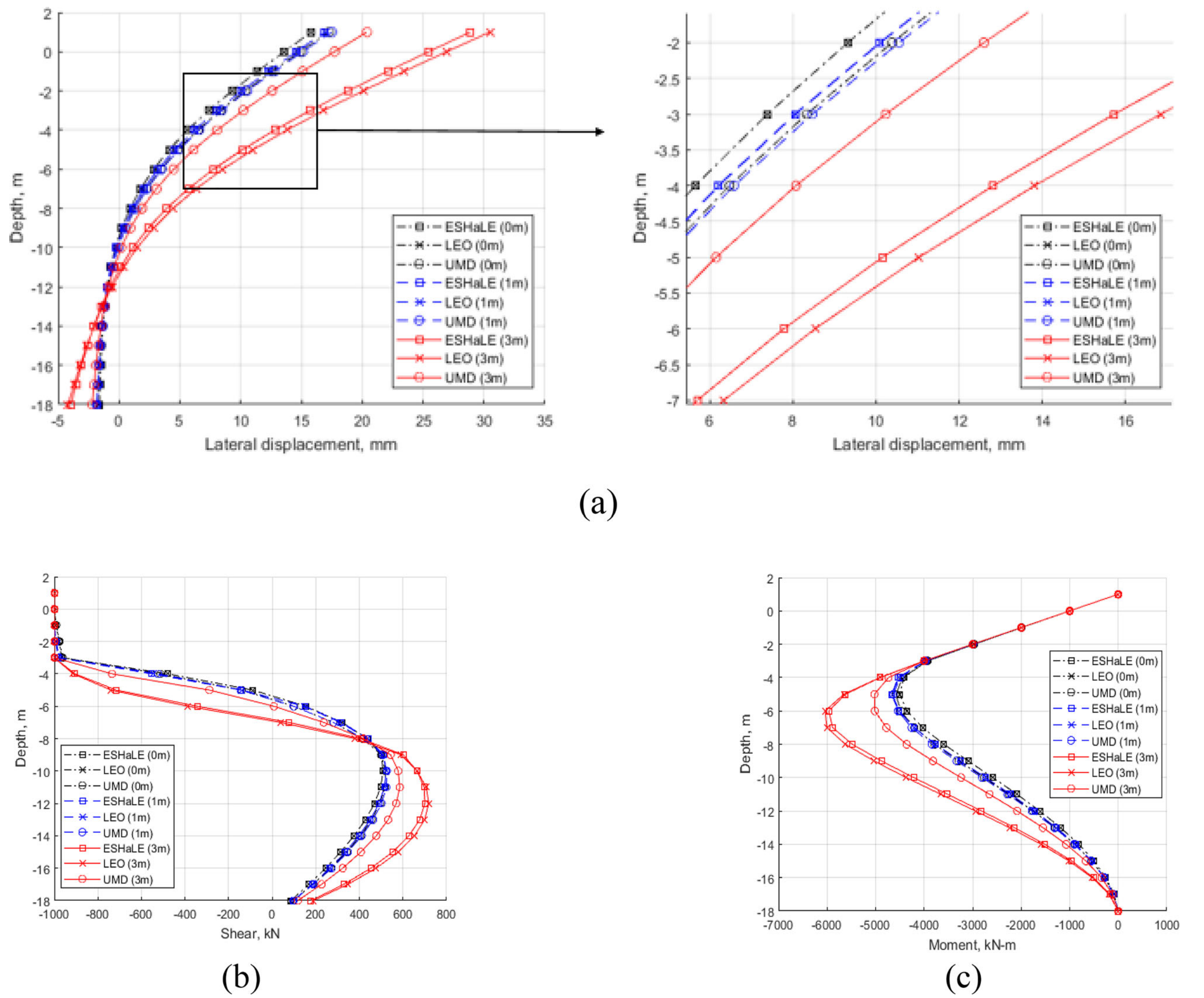

Figure 18. (a) Lateral displacement, (b) shear, and (c) moment diagrams along a single pile considering three soil models and varying scour depths under laterally applied load.

vulnerability of full bridge structures under scour conditions. The impact is investigated considering the dynamic response of a bridge analysed using varying soil models.

5. Bridge evaluation

5.1. Bridge geometry and modeling details

The bridge studied is of a common single-bent concrete box-girder type with integral pier (Mackie & Stojadinovic, 2003). The bridge type is selected for illustrative purposes, and with previous research (Wang et al., 2014) having also used this bridge type for the study of scour phenomenon. The bridge has a span length of 36.6 m and a 2 m wide circular column diameter with height of 10 m. The cross-section of the deck is a 4-cell box girder with reinforced concrete construction with total width of 11 m and depth of 2 m. A Type I pile shaft foundation is used, and the length of the embedded pile shaft is assumed to be 1.75 times the length of the column above grade. Figure 20 shows the longitudinal and transverse views of the selected bridge type. The corresponding dimensions of the bridge are shown in Table 5. Further bridge details can be found in Mackie and Stojadinovic (2003). The soil profile for the bridge evaluation is as shown in Subsection 3.3. The profile consists of three soil layers of soft clay, loose sand, and stiff clay from the top to the bottom.

A finite-element model of the bridge is built in the software OpenSees. For the substructure, the bridge column is modeled using a single force-based element with fiber discretisation in the cross-section. Four integration points along the column are used to capture the flexural response. The ‘Concrete02’ material model is used for the uniaxial constitutive behavior of the concrete, and the confinement effect in the column is captured through special treatment of the stress-strain behavior of the concrete fiber (Mander, Priestley, & Park, 1988). The ‘Steel01’ material model is used for the reinforcement uniaxial material with linear hardening behavior. The pile foundation is implemented using multiple force-based elements with two integrations points (He, Liu, Wang, & Ye, 2016), which consists of the same fiber discretisation as in the column section.

For the superstructure, the deck is modeled using linear elastic beam-column elements. The modeling of the abutment adopts the SDC 2004 abutment model (Mackie & Stojadinovic, 2006), and it is assumed to be a seat-type abutment with an

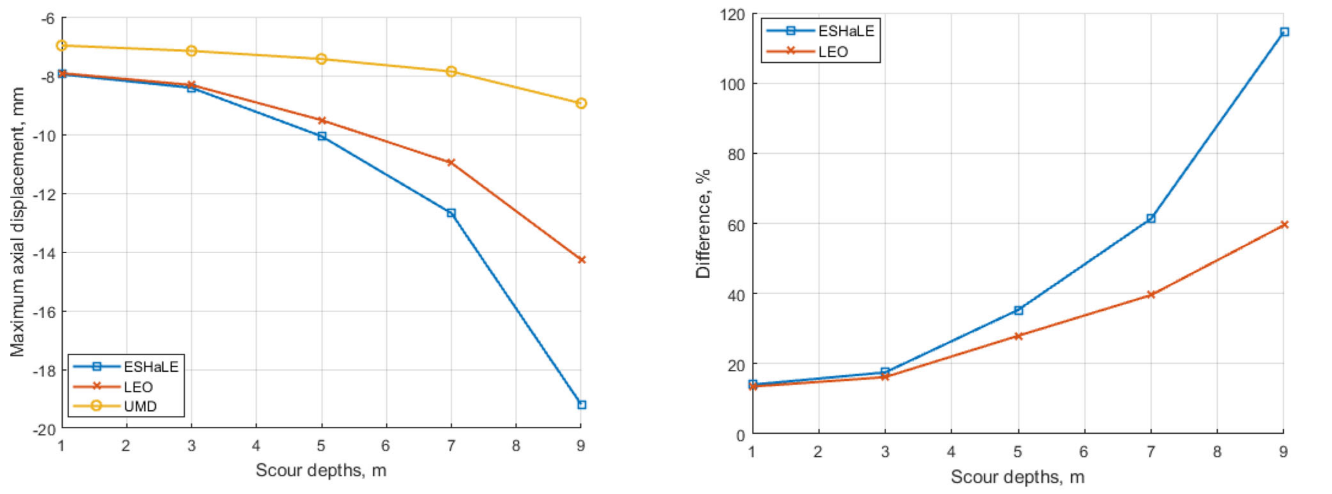

(a) (b)

Figure 19. (a) Comparison of maximum axial displacement of single pile between ESHaLE, LEO, and UMD models at varying scour depths and (b) percentage difference between the three models.

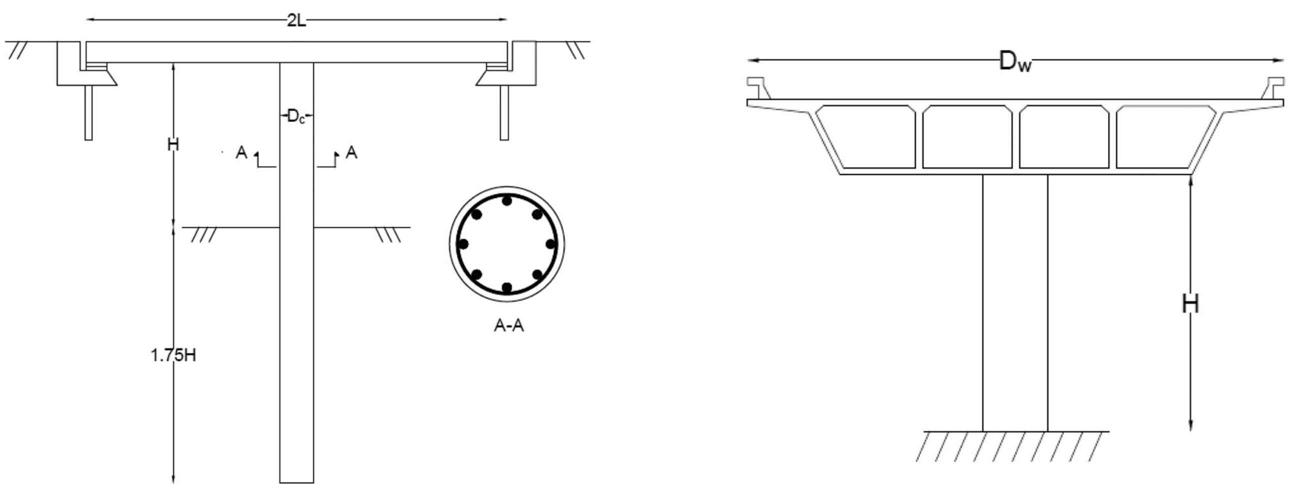

(a) (b)

Figure 20. (a) Longitudinal view of single-frame box-girder concrete bridge and (b) transverse view.

Table 5. Geometric parameters of the selected bridge.

	Span Length (L), m	Column height(H), m	Column diameter ($\mathbf{D_c}$), m	Deck width ($\mathbf{D_w}$), m
Single-bent box-girder bridge	36.6	10.0	2.0	11

initial gap of about 150 mm (Priestley, Seible, & Calvi, 1996). The abutment model consists of longitudinal, transverse, and vertical nonlinear abutment responses. In particular, the longitudinal system response considers the responses of the elastomeric bearing, gap, abutment pile, backfill material, and impact between the deck and abutment backwall. The transverse response considers system responses of the elastomeric bearing, wing walls, abutment piles, and backfill material. The vertical response of the abutment model is assumed to be affected by the vertical stiffness of the bearing pad only. Two bearing pad springs with 50 mm depth (Mackie & Stojadinovic, 2003) have also been added to the bridge models. The modeling of the elastomeric bearing uses nonlinear springs with perfectly plastic behavior, and yield displacement of the bearings is assumed to be at 150% of the shear strain.

The modeling of soil–structure interaction (SSI), as shown in Figure 17(b), is implemented using the dynamic *p-y* method to explicitly account for SSI effects while maintaining an acceptable computing time for probabilistic analyses (Wang et al., 2014). The nonlinear *p-y* and *q-z* behaviors are conceptualised as consisting of elastic, plastic, and gap components in series; the nonlinear *t-z* behavior is conceptualised as consisting of elastic and plastic components in series. Further details regarding this method can be found in Boulanger, Curras, Kutter, Wilson, and Abghari (1999). The foundation pile is modeled as a beam on a

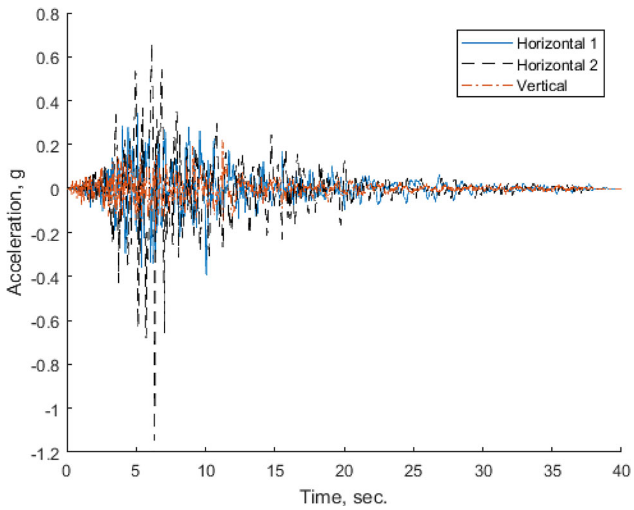

Figure 21. Three components of the selected ground motion.

nonlinear Winkler foundation. Lateral SSI is captured by a *p-y* spring, while vertical axial friction and tip bearing capacity are captured by *t-z* and *q-z* springs, respectively. This study assumes stiff clay and soft clay share the same *p-y* relation due to the limited set of *p-y* relations implemented in OpenSees, and the fact that the *p-y* relation for stiff clay without free water does not soften after reaching peak stress (Welch & Reese, 1972). Note that the proposed ESHaLE framework will be valid regardless of the modeled behavior of the soil *p-y* relation. In specifying the soil spring properties, the three varying soil models (ESHaLE, LEO, and UMD) are implemented in OpenSees to capture differences in the soil response.

5.2. Seismic response of bridge with layered soils

To assess the bridge response in detail, this section presents the seismic response of the bridge under a particular ground motion shown in Figure 21. Fragility assessment of the bridge under a suite of ground motions is presented in the following section. The ground motion is selected from the PEER database (Baker, Lin, Shahi, & Jayaram, 2011) with two horizontal components and one vertical component as shown in Figure 21. The ground motion name is Loma Prieta with a magnitude of 6.93 and shear wave velocity in the top 30 m of 489 m/s. The seismic analysis is implemented through a uniform input across the soil depth (Shang, Alipour, & Ye, 2018). Five levels of scour are considered for this section: scour depths of 1 m, 3 m, 5 m, 7 m, and 9 m. Nonlinear response history analyses are run and performance of critical bridge elements are evaluated. The critical responses include the vertical displacement of the column, the curvature distribution of the bridge column, and the transverse and longitudinal deck displacements.

Excessive vertical displacement of column could lead to local failure of the bridge deck due to concrete crushing in the compression region. Figure 22 presents the maximum vertical displacement of the column at each scour depth from using the three soil models. From Figure 22, when the scour depth is less than 3 m, the LEO model exhibits slightly larger vertical displacements among the three soil models because the stress history effect of sand becomes the governing factor, increasing the vertical resistance. However, the trend changes at higher scour depths. From Figure 22(b), looking over the full time history, there is an increase of 16% and 10% in calculated vertical displacement between the ESHaLE and UMD, and LEO and UMD models, respectively. These values indicate the underestimation in the estimation of the vertical displacement response possible if analyses do not properly account for both the stress history and layered soil effects.

Figure 23 presents the maximum curvature distribution along the column and pile for the five different scour levels. The curvature distribution shown in Figure 23 accounts for both the transverse and longitudinal directions through their geometric mean. Excessive curvature demand could lead to flexural failure of the column. The results in Figure 23 lead to several observations. First, the maximum curvature distribution of the ESHaLE model and LEO models are close to each other regardless of changes in scour depth, implying that the stress history effect has a limited influence on the lateral behavior of the vertical element. Second, due to the layered effect, the maximum curvature distributions of the ESHaLE and LEO models begin to deviate from the UMD model from a scour depth of 3 m onward. The maximum curvature distribution changes by decreasing the relative curvature at the top of the column as well as the portion below mudline level for the ESHaLE and LEO models compared with UMD model. This is because the redistribution of forces along the pile due to the change of soil stiffness influences the deformation of the structural member. Third, the largest maximum curvature demand always occurs in the UMD model due to the stiffer soil model without accounting for the layered soil effects. Fourth, the magnitude of the maximum curvature distribution for all three cases decreases as scour depth increases due to the lengthening of the structural period and reduction of seismic force attracted. In addition to the maximum curvature distributions, Figure 24 presents hysteresis loops at the top of bridge column where maximum curvature occurs considering the three different models. Figure 24 shows both transverse and longitudinal moment-curvature responses of the column. The results are consistent with those from Figure 23 showing inelastic behaviors and the largest value of curvature occurring in the UMD model.

Finally, the horizontal displacement of the deck is also evaluated. Excessive displacement of the deck at the seat abutments could lead to unseating of the bridge deck. For brevity, the time-history responses of the bridge deck for only two levels of scour of 5 m and 9 m are shown in the transverse (Figures 25(a,b)) and longitudinal (Figure 25(c,d)) directions, respectively. From Figure 25, one observes that first, there is only a small difference in terms of maximum displacement exhibited among the three soil models, especially in the longitudinal direction. Second, the lower scour level (i.e. 5 m) leads to a higher displacement demand in comparison with the higher scour level (i.e. 9 m) in the transverse direction. This is due to the increasing structural period with scour depth, decreasing the attraction of seismic force at higher scour

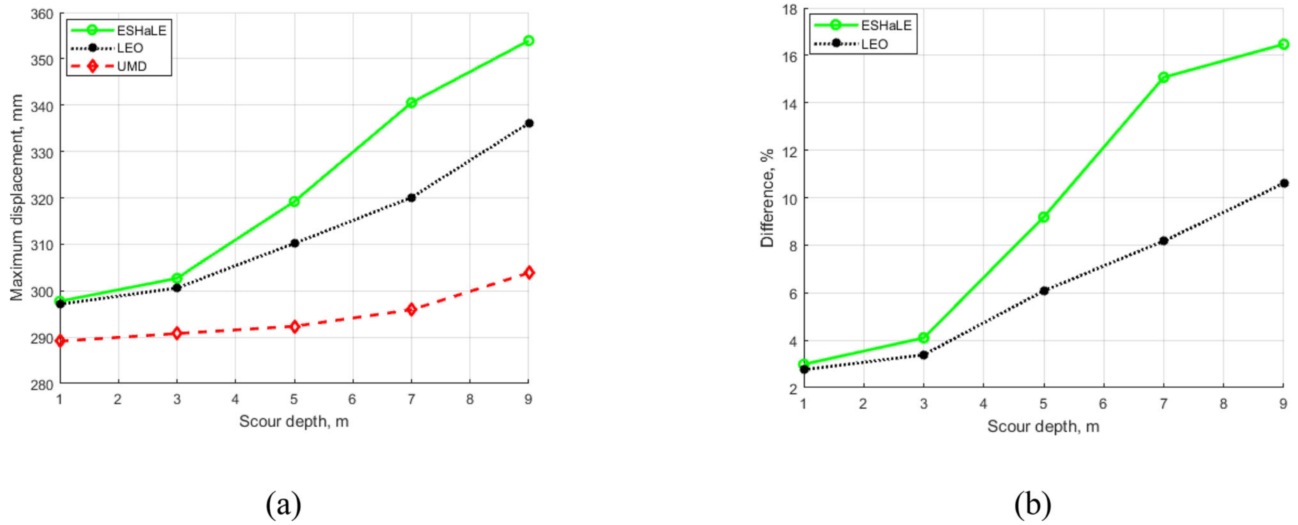

Figure 22. (a) Maximum vertical displacement of column for varying scour depths considering three soil models and (b) percentage differences between ESHaLE versus UMD models and LEO versus UMD models.

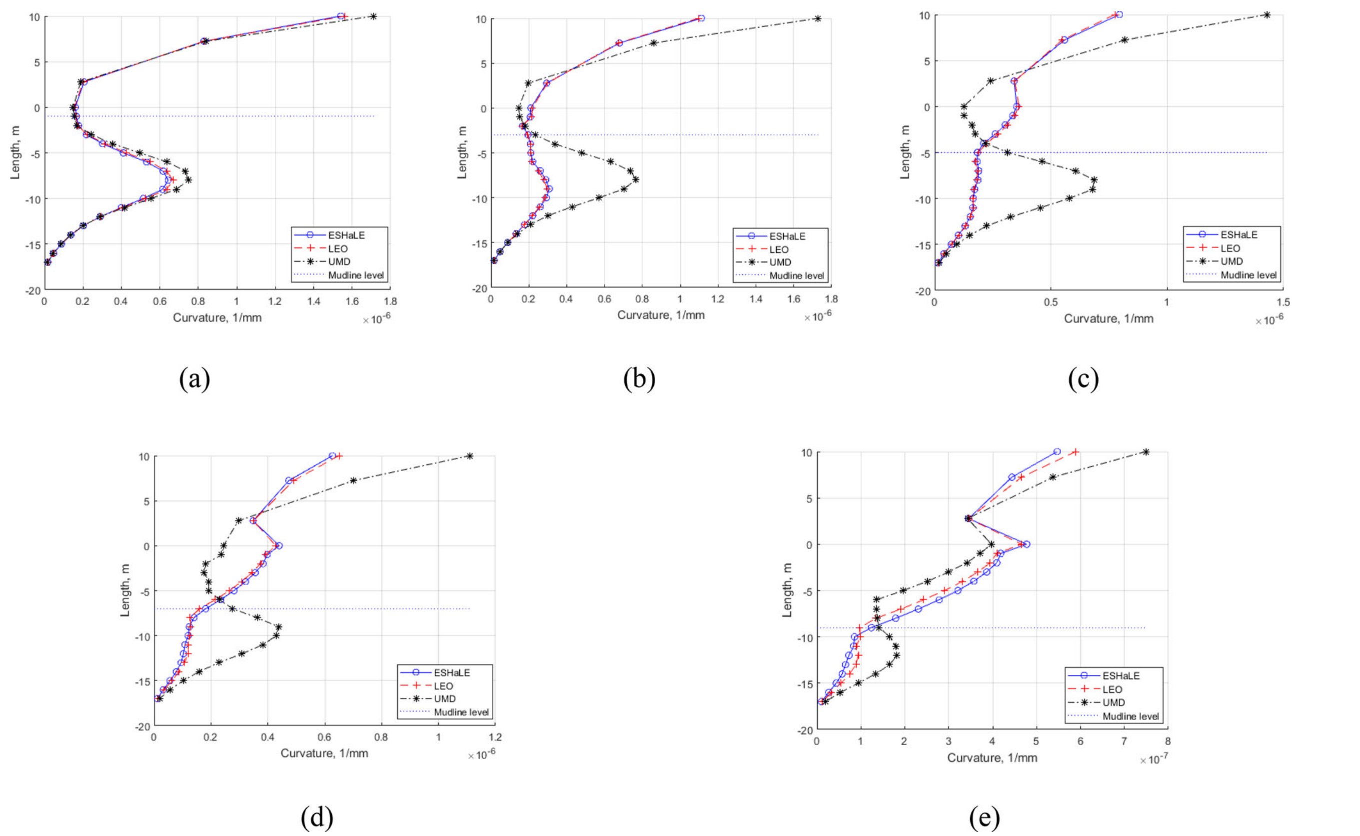

Figure 23. Curvature envelope along column and foundation pile using the three soil models considering (a) 1 m, (b) 3 m, (c) 5 m, (d) 7 m, and (e) 9 m scour depths.

levels. Third, while a residual displacement is observed from the time-history response of the deck in the transverse direction, with the UMD model resulting in a higher residual displacement than the other two models, after an investigation of the residual displacement of the bridge deck considering multiple ground motions, the authors have found that the difference of residual displacement among the three models is due to several factors, including characteristics of the ground motion, soil modeling, and scour level. The next section provides an assessment of the three soil models considering multiple ground motions using fragility analyses.

5.3. Fragility assessment of bridges with layered soils

A total of 59 ground motions with two horizontal components and one vertical component are considered for fragility assessment. The ground motion suite is chosen from the PEER database (Baker et al., 2011), and the spectral accelerations for all three components are shown in Figure 26. Note that the current study only focuses on uncertainty in ground motions with the assumption that the same uncertainties exist between the proposed and existing models because the goal of the study is to present a new soil model

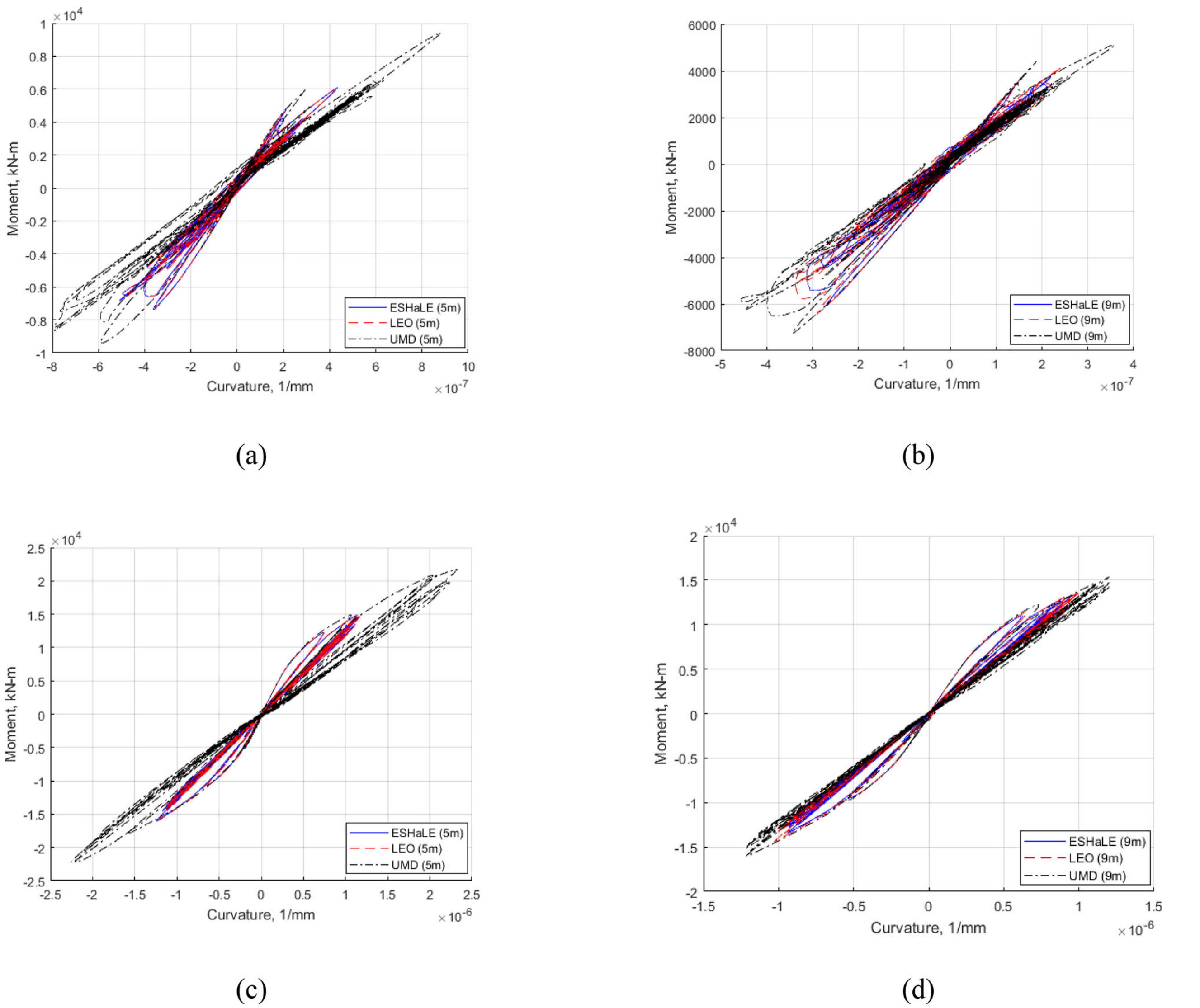

Figure 24. Moment-curvature responses of the column in (a) & (b) transverse and (c) & (d) longitudinal directions for scour levels of (a) & (c) 5 m and (b) & (d) 9 m.

(ESHaLE) that is capable of capturing the impact of stress history of the layered soil in both lateral and vertical directions. The uncertainties associated with the soil profile, e.g. layer thickness, soil composition, etc., as well as uncertainties in the soil properties will influence the bridge fragility assessment. However, these analyses, including the effects of uncertainties, are outside the scope of the current study and would be an interesting topic for future studies on bridge performance.

Here, analytical fragility curves are computed through running a series of nonlinear time history analyses on deterministic bridges. A number of previous studies have adopted this methodology for fragility assessment (Choi et al., 2004; Nielson & DesRoches, 2007; Padgett, 2007; Zhang, DesRoches, & Tien, 2019a). The uncertainty considered in this fragility assessment is in variation of ground motions. The column fragility is expressed as the probability of exceeding some damage state for a specific intensity measure. This probability of failure P_f can be expressed as a function of parameters of the capacity and demand variables assuming both follow a lognormal distribution as shown in Equation (16).

$$P_f = \Phi\left(\frac{\ln S_d/S_c}{\sqrt{\xi_d^2 + \xi_c^2}}\right) \tag{16}$$

$\Phi(\cdot)$ is the standard normal cumulative distribution function. S_d and S_c are the median parameters for the demand and capacity distributions, respectively, and ξ_d and ξ_c are the lognormal standard deviation of the demand and capacity distributions, respectively.

Following the findings from the previous section, the engineering demand parameters are selected to be the vertical displacement and curvature ductility of the column. As the ESHaLE model results in a reduced curvature demand in comparison with the UMD model as shown in Figure 23, column curvature is expected to yield a decreased curvature demand in comparison with the UMD model. The effect of stress history of layered soils has a less significant impact on the curvature demand due to a large portion of bridge lateral stiffness being contributed to from the abutments. In terms of lateral bridge performance, a curvature ductility (μ_ϕ) value of 12 is selected to be a threshold value to describe flexural failure of the column due to buckling of the longitudinal reinforcement in post-

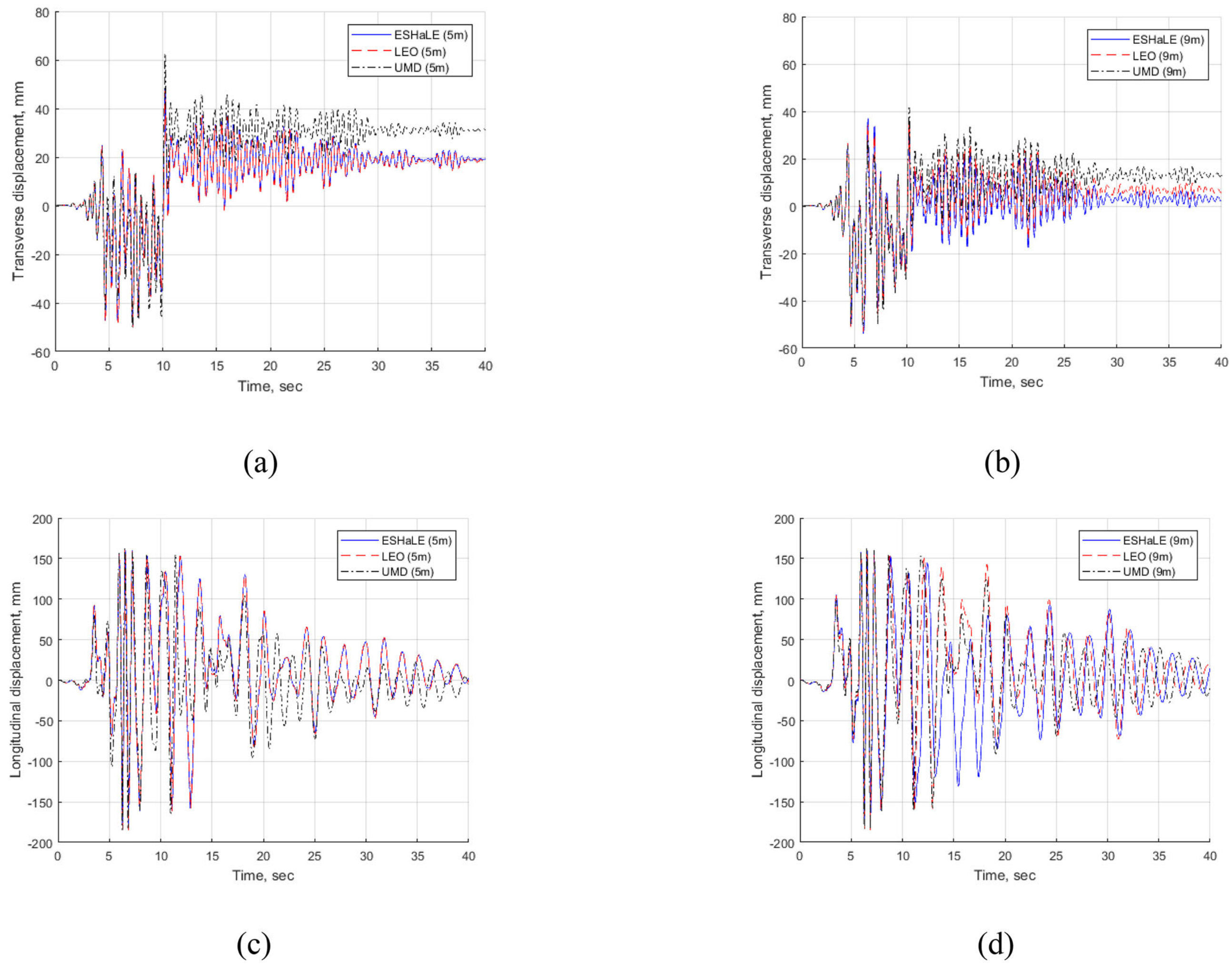

Figure 25. Time history response of deck (a) & (b) transverse and (c) & (d) longitudinal displacement for scour levels of 5 m and 9 m.

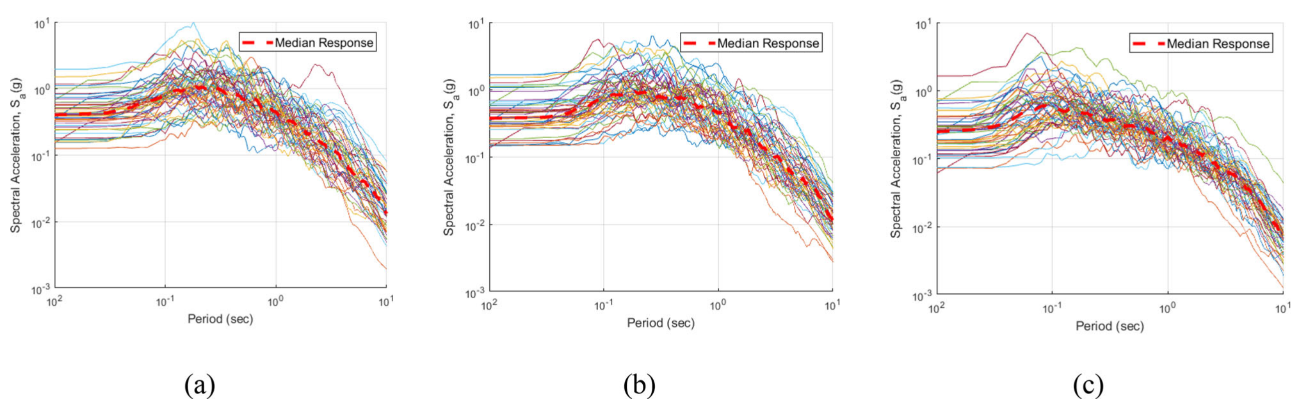

Figure 26. Spectral accelerations of ground motion suite for (a) horizontal component one, (b) horizontal component two, and (c) vertical component.

1990s bridge designs (Ramanathan, 2012). Note that shear failure of the bridge column is not considered in this study as it is less likely to occur for this bridge type where the column and pile shaft share the same cross section. Increasing the unbraced length due to scour leads to a larger shear span to depth ratio, which could increase flexural cracking and reduce shear strength (Sezen & Moehle, 2004). However, the reduction of seismic demand due to scour for this bridge type (Zhang, DesRoches, & Tien, 2019b) decreases the probability of occurrence of shear failure.

In terms of performance of the bridge deck, bridge deck deflection limits are considered. Aashto (2012) defines a serviceability limit of L/800 for the bridge deck deflection. Assuming the bridge deflection limit goes beyond the serviceability limit, this study uses L/250 as the threshold for fragility assessment. This value is selected based on previous studies of bridge inspections (Roeder et al., 2002). In that study, the largest deflection measured among inspected bridges after applying HS20-44 standard truck loading was a critical deflection of L/264 in the center span as experienced

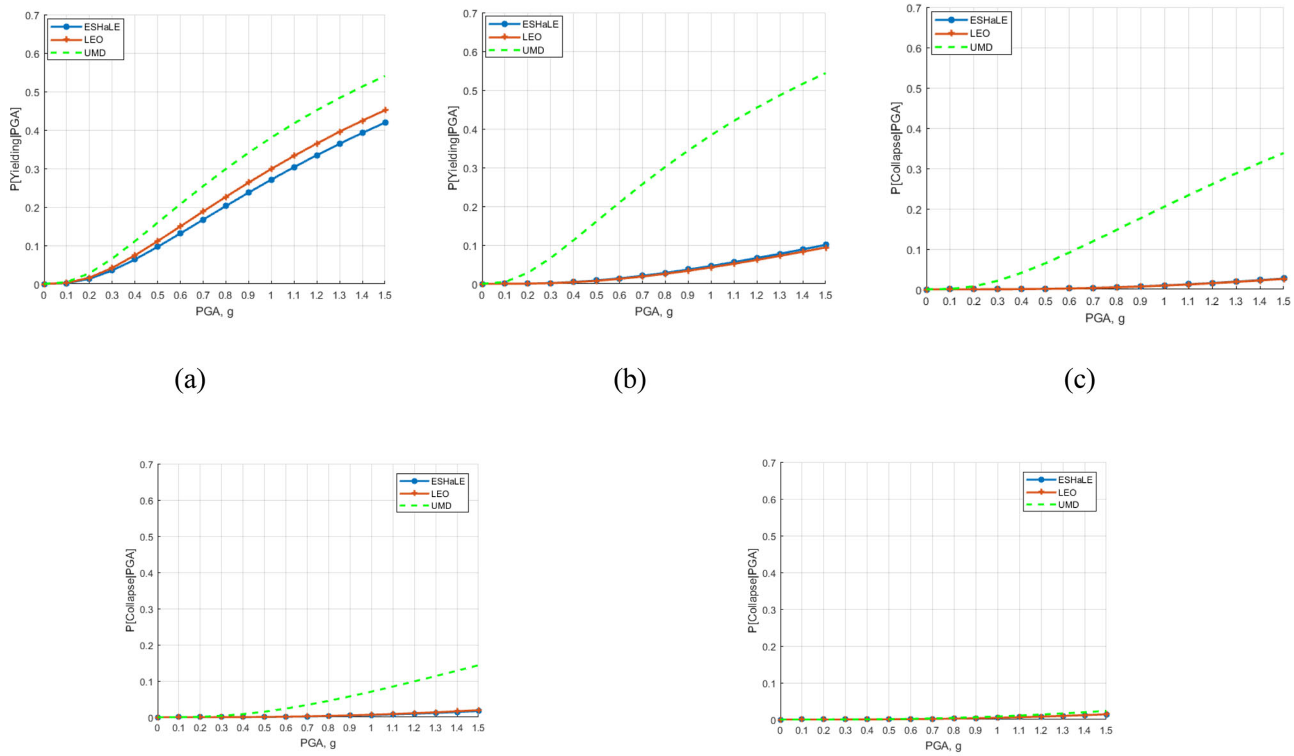

(a) (b) (c)

(d) (e)

Figure 27. Probability of exceeding flexural failure of bridge column using the three soil models for (a) 1 m, (b) 3 m, (c) 5 m, (d) 7 m, and (e) 9 m scour levels.

by the US-50 bypass bridge. As such, a similar value is used as a benchmark to evaluate the bridge deck deflection under a larger loading. Note that other limit states can also be chosen. For example, the bridge deck can be modeled with nonlinear elements to capture nonlinear behavior of the bridge deck and an instance of material failure (i.e. crushing of concrete or buckling of reinforcement). Such limit states can be defined and the proposed ESHaLE method can be applied for analysis without loss of generality.

Fragility curves for column lateral performance are shown in Figure 27 for 1 m, 3 m, 5 m, 7 m, and 9 m scour depths. Based on the results, the failure probabilities obtained from all three models are consistent with results presented previously. The results show the following: first, as scour levels increase, the probabilities of exceeding the collapse damage state for all three models decrease. This is because for this bridge type, the removal of soil springs due to scour lengthens the fundamental period of the bridge, reducing the seismic demand (e.g. the curvature ductility demand) and acting as a base isolation in the presence of a more flexible foundation system. This phenomenon is also observed in Wang et al. (2014). The decrease in failure probability can also be due to the characteristics of the selected bridge type. In contrast to having a relatively flexible connection (i.e. elastomeric bearing) between the bridge deck and column, the integral connection enables the superstructure and substructure to act as a whole and restrains the column from displacing excessively under scour conditions. A different soil type could also influence the bridge response by providing different stiffness in the presence of scour. Second, the results show that the UMD model yields the highest failure probabilities among the three models across all scour levels. This is because the UMD model produces stiffer soil springs as it is accompanied by a higher value of lateral resistance as shown in Figure 8, resulting in attracting a larger seismic demand. Third, by comparing the fragility curves between the ESHaLE and LEO models, the impact of stress history is more influential at low scour levels (e.g. 1 m) with a slightly higher failure probability from the LEO model because the low scour level is accompanied by attraction of a higher seismic force. The impact of stress history of layered soils on lateral bridge performance is minimal at higher scour levels.

Figure 28 presents the demand distribution of bridge deck deflections as a function of peak ground acceleration (PGA) for 1 m, 3 m, 5 m, 7 m, and 9 m sour levels after performing 59 nonlinear time history analyses for each scour depth. Figure 29 summarises the mean values from Figure 28 and shows that the proposed model exhibits the highest deflection among the three models. There is a maximum increase of 16% and 8% between the ESHaLE and UMD models and between the LEO and UMD models, respectively. The ESHaLE model results in a larger increase in the mean value of the deck deflection due to the fact that as scour depth increases, the contribution of side friction reduces due to the removal of *t-z* springs, which in turn increases the contribution of the tip resistance. As a result, based on Figure 12, at larger scour depths, the ESHaLE

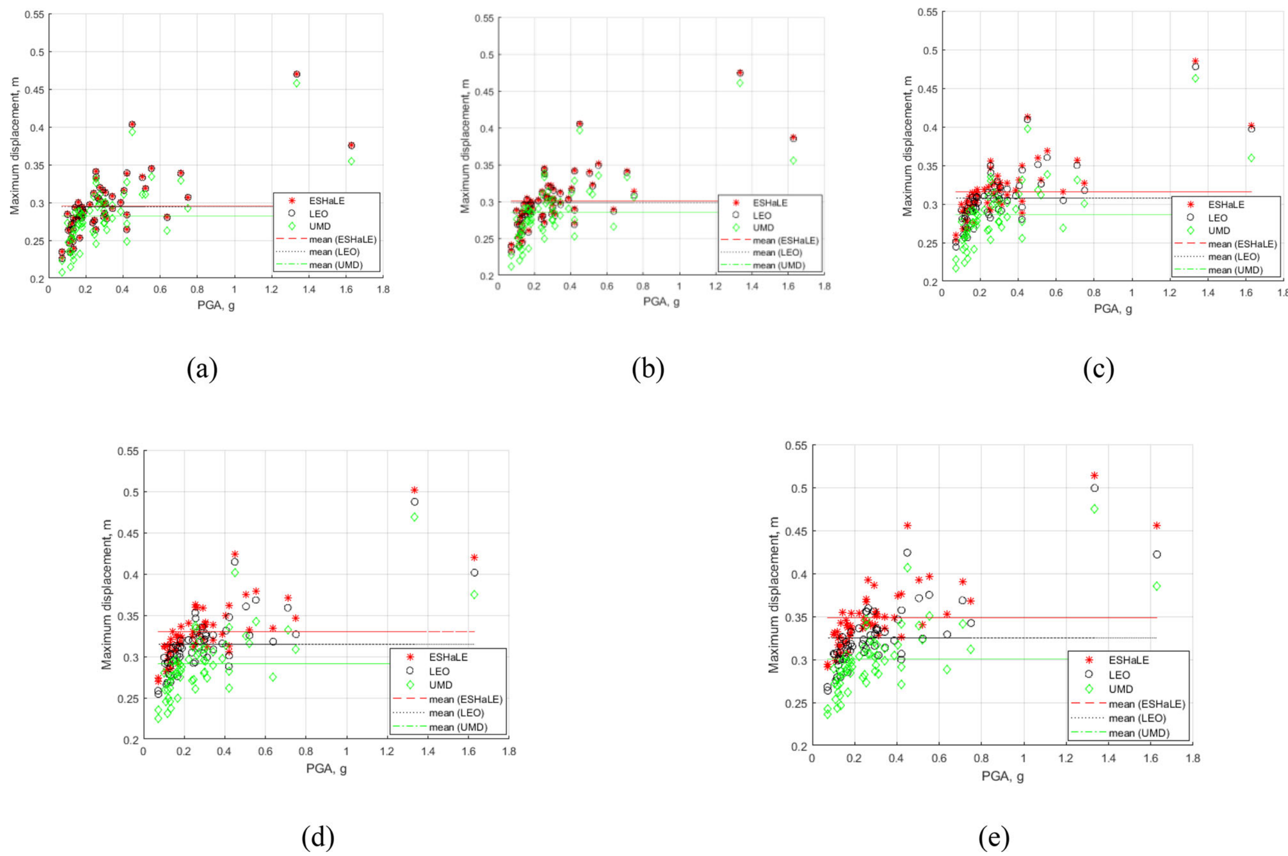

Figure 28. Maximum vertical displacement of bridge deck versus PGA for (a) 1 m, (b) 3 m, (c) 5 m, (d) 7 m, and (e) 9 m scour depths.

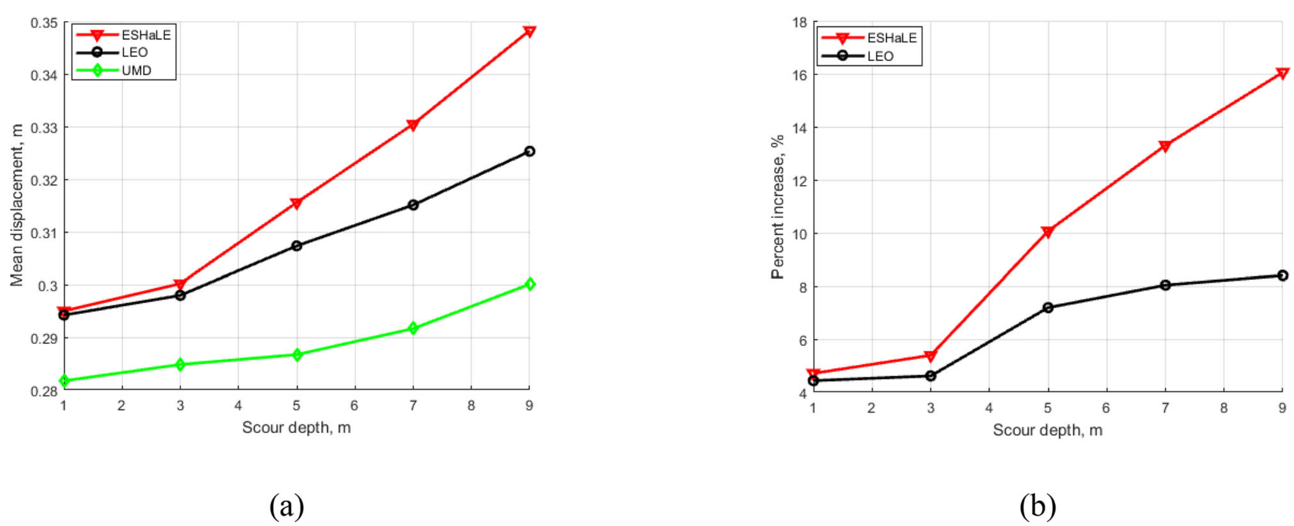

Figure 29. (a) Mean deflections of bridge deck versus scour depth and (b) percent increase between the ESHaLE and UMD and LEO and UMD models.

model has lower resistance in comparison with the other models.

Fragility curves for vertical displacement of the column are presented in Figure 30 for 1 m, 3 m, 5 m, 7 m, and 9 m scour depths. The results from the fragility assessment are consistent with the component-level column vertical displacement responses presented in Figure 22. When the scour depth is less than 5 m, the LEO model results in a higher probability of exceedance as the stress history effect of the sand layer increases the vertical resistance of the soil. However, when the scour depth is 5 m or larger, the ESHaLE model yields a higher probability of exceedance. Figure 31 presents the probability differences among the three soil models based on the results shown in Figure 30. Figure 31(a) gives the probability difference between the ESHaLE and LEO models, with a maximum probability difference of around 25% at 9 m scour depth. Figure 31(b) gives the probability difference between the ESHaLE and UMD models, with a maximum probability difference of around 46% at 9 m scour depth. Both Figure 31(a,b) show that the impact of including the stress history effect in bridge vulnerability assessment is magnified and becomes more critical as scour depth increases.

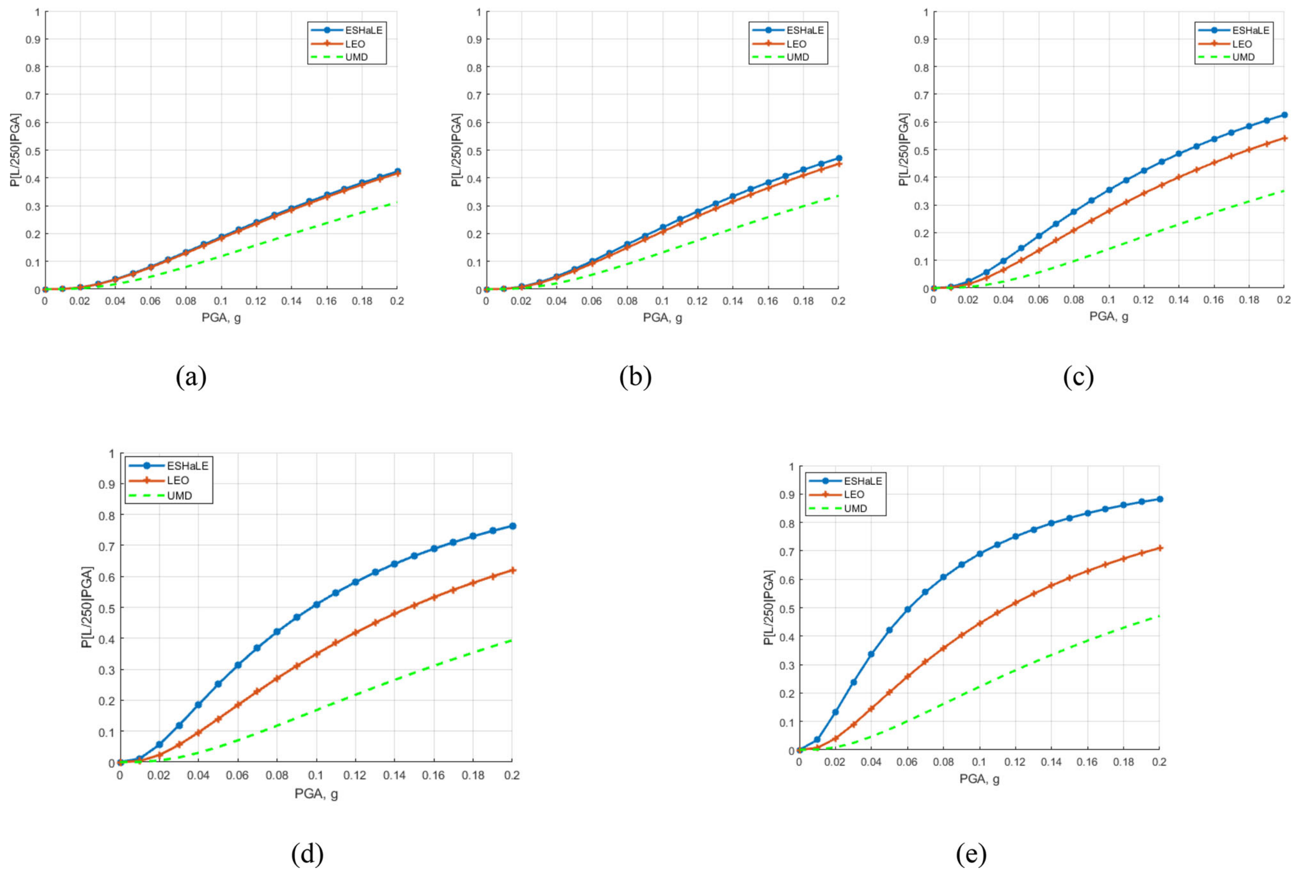

Figure 30. Probability of exceeding L/250 deflection of bridge deck using the three soil models for (a) 1 m, (b) 3 m, (c) 5 m, (d) 7 m, and (e) 9 m scour levels.

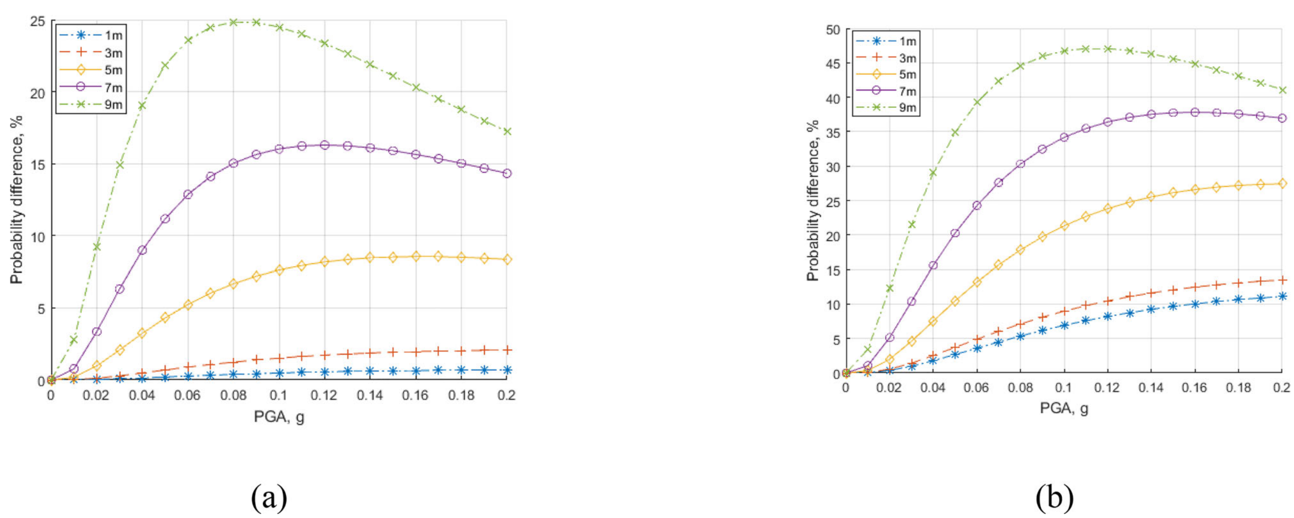

Figure 31. Probability differences between ESHaLE model and (a) LEO model and (b) UMD model in terms of probability of exceeding L/250 deflection threshold.

6. Conclusions

This study proposes a new methodology called the ESHaLE approach to account for the effect of stress history in soil profiles with multiple layers, including both sandy and clayey soils. The theoretical basis of ESHaLE model consists of two main aspects. First, the impact of stress history on the behavior of soils is captured based on conservation of mass under a general scour scenario. Second, to accommodate the special characteristic of layered soils, the layered effect is also included in the ESHaLE model based on conservation of strength for the lateral response and continuity of effective vertical stress for the vertical response. The conservation of mass along with the conservation of strength are used to find equivalent layers and corresponding equivalent layer depths, scour depths, and soil properties for vulnerability assessment of scoured bridges. The methodology is verified through comparison with both existing models and experimental tests. ESHaLE is evaluated on an example soil profile, and implemented on a laterally and vertically loaded pile for a static analysis as well as a full bridge structure for a dynamic analysis with the goal of assessing seismic vulnerability under scour conditions. Three soils models are compared: the proposed ESHaLE model that is able to capture both the stress history and layered soil effects, the LEO model that includes the layered effect only, and the UMD model that represents the unmodified soil model and ignores both the layered and stress history effects. The main findings based on the results from the single pile test and the seismic vulnerability analyses of the bridge considering the three soil models are as follows:

- The results from the laterally and vertically loaded pile show that the impact of stress history on the lateral response of the pile increases as scour level increases. For the vertically loaded pile, using the proposed ESHaLE model results in the largest value of axial displacement among the three models with a maximum increase of 35% in comparison with the LEO model due to stress history effects on the structural response.
- From the results from a selected ground motion, an increase of up to 10% and 16% in terms of column vertical displacement is observed in using the proposed ESHaLE model compared with the LEO and UMD models, respectively. Importantly, as scour depth increases, column vertical displacements obtained from using the ESHaLE model are amplified in comparison with the values from the LEO or UMD models.
- From the fragility assessments for flexural failure of the bridge column, the failure probabilities obtained from implementing the proposed ESHaLE model compared with the LEO model show the impact of stress history is more significant at low scour levels due to the attraction of higher seismic force in comparison with results for higher scour levels
- From the fragility curves, using the ESHaLE soil model results in a 25% and 46% higher probability that the deflection of the deck will exceed a L/250 threshold in comparison with the LEO and UMD models, respectively. The increase in estimated exceedance probability increases as scour depth increases.
- Taken together, these findings show the importance of implementing a modeling approach as proposed with ESHaLE that includes the effect of soil stress history to assess the vulnerability of scoured bridges in layered soils.

Disclosure statement

No potential conflict of interest was reported by the authors.

Funding

This project was partially funded by the INSPIRE University Transportation Center (UTC). Financial support for INSPIRE UTC projects is provided by the U.S. Department of Transportation, Office of the Assistant Secretary for Research and Technology (USDOT/OST-R) under Grant No. 69A3551747126 through INSPIRE University Transportation Center (http://inspire-utc.mst.edu) at Missouri University of Science and Technology. The views, opinions, findings and conclusions reflected in this publication are solely those of the authors and do not represent the official policy or position of the USDOT/OST-R, or any State or other entity.

References

Aashto, L. (2012). *AASHTO LRFD bridge design specifications*. Washington, DC: American Association of State Highway and Transportation Officials.

Alipour, A., Shafei, B., & Shinozuka, M. (2013). Reliability-based calibration of load and resistance factors for design of RC bridges under multiple extreme events: Scour and earthquake. *Journal of Bridge Engineering*, *18*, 362–371. doi:10.1061/(ASCE)BE.1943-5592.0000369

API RP 2A. (2000). Recommended Practice for Planning, Designing and Constructing Fixed Offshore Platforms—Working Stresses Design, 21st Edition American Petroleum Institute, Washington.

Aygun, B. (2009). *Efficient seismic fragility assessment of highway bridges on liquefiable soils* (Master thesis). Rice University.

Baker, J. W., Lin, T., Shahi, S. K., & Jayaram, N. (2011). *New ground motion selection procedures and selected motions for the PEER transportation research program.* PEER Report (2011/3).

Banerjee, S., & Ganesh Prasad, G. (2013). Seismic risk assessment of reinforced concrete bridges in flood-prone regions. *Structure and Infrastructure Engineering*, *9*, 952–968. doi:10.1080/15732479.2011.649292

Boulanger, R. W., Curras, C. J., Kutter, B. L., Wilson, D. W., & Abghari, A. (1999). Seismic soil-pilestructure interaction experiments and analyses. *Journal of Geotechnical and Geoenvironmental Engineering*, *125*, 750–759. doi:10.1061/(ASCE)1090-0241(1999)125:9(750)

Brown, D. A., & Castelli, R. J. (2010). "Construction procedures and LRFD design methods." Rep. FHWA-NHI-10-016, Federal Highway Administration, Washington, DC.

Cairo, R., & Conte, E. (2006). Settlement analysis of pile groups in layered soils. *Canadian Geotechnical Journal*, *43*, 788–801. doi:10.1139/t06-038

Choi, E., DesRoches, R., & Nielson, B. (2004). Seismic fragility of typical bridges in moderate seismic zones. Engineering structures, 26(2), 187–199.

Cox, W. R., Reese, L. C., & Grubbs, B. R. (1974). *Field testing of laterally loaded piles in sand*. Presented at the Offshore Technology Conference. Offshore Technology Conference. doi:10.4043/2079-MS

Davisson, M. T., & Gill, H. L. (1963). Laterally loaded piles in a layered soil system. *Journal of the Soil Mechanics and Foundations Division*, *89*, 63–94.

Fioklou, A., & Alipour, A. (2019). Significance of non-uniform scour on the seismic performance of bridges. *Structure and Infrastructure Engineering*, *15*, 822–836. doi:10.1080/15732479.2019.1584226

Gazetas, G., & Dobry, R. (1984). Horizontal response of piles in layered soils. *Journal of Geotechnical Engineering*, *110*(1), 20–40. doi:10.1061/(ASCE)0733-9410(1984)110:1(20)

Georgiadis, M. (1983, April). Development of py curves for layered soils. In *Geotechnical practice in offshore engineering* (pp. 536–545). ASCE.

Georgiadis, M., Anagnostopoulos, C., & Naskos, N. (1999). *Effect of pile-head enlargement on lateral and axial responses of a bored pile*. Presented at the International Conference on Soil Mechanics and Foundation Engineering (pp. 809–812).

He, Z., Liu, W., Wang, X., & Ye, A. (2016). Optimal force-based beam-column element size for reinforced-concrete piles in bridges. *Journal of Bridge Engineering*, *21*, 06016006. doi:10.1061/(ASCE)BE.1943-5592.0000926

Huang, M., Liang, F., & Jiang, J. (2011). A simplified nonlinear analysis method for piled raft foundation in layered soils under vertical loading. *Computers and Geotechnics*, *38*, 875–882. doi:10.1016/j.compgeo.2011.06.002

Lagasse, P. F., Clopper, P. E., Zevenbergen, L.W., & Girard, L.W. (2007). *Countermeasures to protect bridge piers from scour. NCHRP Rep.* (Vol.

593). Washington, DC: National Cooperative Highway Research Program, Transportation Research Board, National Academies.

Lin, C., Bennett, C., Han, J., & Parsons, R. L. (2010). Scour effects on the response of laterally loaded piles considering stress history of sand. *Computers and Geotechnics*, *37*, 1008–1014. doi:10.1016/j.compgeo.2010.08.009

Lin, C., Han, J., Bennett, C., & Parsons, R. L. (2014). Behavior of laterally loaded piles under scour conditions considering the stress history of undrained soft clay. *Journal of Geotechnical and Geoenvironmental Engineering*, *140*, 06014005. doi:10.1061/(ASCE)GT.1943-5606.0001112

Mackie, K., & Stojadinovic, B. (2003). *Seismic demands for performance-based design of bridges*. Berkeley: Pacific Earthquake Engineering Research Center.

Mackie, K., & Stojadinovic, B. (2006, September 18–20). *Seismic vulnerability of typical multi-span california highway bridges*. Presented at the Proceedings of the Fifth National Seismic Conference on Bridges and highways, San Francisco.

Mander, J. B., Priestley, M. J., & Park, R. (1988). Theoretical stress-strain model for confined concrete. *Journal of Structural Engineering*, *114*, 1804–1826. doi:10.1061/(ASCE)0733-9445(1988)114:8(1804)

Matlock, H. (1970). *Correlation for design of laterally-loaded piles in soft clay*. Presented at the Proceedings of the 2nd *Annual Offshore Technology Conf*erence (pp. 277–594), American Institute of Mining, Metallurgical, and Petroleum Engineers, Houston.

Mayerhof, G. G. (1976). Bearing capacity and settlement of pile foundations. Journal of the Geotechnical Engineering Division, 1976, Vol. 102, Issue 3, Pg. 197–228

McKenna, F. T. (1997). *Object-oriented finite element programming: Frameworks for analysis, algorithms and parallel computing* (Doctoral dissertation). University of California at Berkeley, Berkeley, CA

Mosher, R. L. (1984). Load-Transfer Criteria for Numerical Analysis of Axially Loaded Piles in Sand. Part 1. Load-Transfer Criteria (No. WES-TR-K-84-1). ARMY ENGINEER WATERWAYS EXPERIMENT STATION VICKSBURG MS.

Nielson, B. G., & DesRoches, R. (2007). Analytical seismic fragility curves for typical bridges in the central and southeastern United States. Earthquake Spectra, 23(3), 615–633.

Padgett, J. E. (2007). *Seismic vulnerability assessment of retrofitted bridges using probabilistic methods* (Ph.D. dissertation). Georgia Institute of Technology, Atlanta, GA

Priestley, M. J. N., Seible, F., & Calvi, G. M. (1996). *Seismic design and retrofit of bridges*. New York, NY: Wiley.

Ramanathan, K. N. (2012). *Next generation seismic fragility curves for California bridges incorporating the evolution in seismic design philosophy* (Doctoral dissertation). Georgia Institute of Technology.

Reese, L. C., Cox, W. R., & Koop, F. D. (1974). *Analysis of laterally loaded piles in sand* (pp. 95–105). Offshore Technology in Civil Engineering Hall of Fame Papers from the Early Years.

Reese, L. C., & O'Neill, M. W. (1987). *Drilled shafts: Construction procedures and design methods, Report No. FHWA-HI-88-042*. Virginia: US Department of Transportation, Federal Highway Administration.

Reese, L. C., & Welch, R. C. (1975). Lateral loading of deep foundations in stiff clay. *Journal of Geotechnical and Geoenvironmental Engineering*, *101*.

Reese, L. C., and Van Impe, W. F. (2001). Single piles and pile groups under lateral loading, Balkema, Leiden, Netherlands.

Roeder, C. W., Barth, K., Bergman, A., & Christopher, R. A. (2002). Improved live load deflection criteria for steel bridges. Transportation Research Board, National Research Council.

Sezen, H., & Moehle, J. P. (2004). Shear strength model for lightly reinforced concrete columns. *Journal of Structural Engineering*, *130*, 1692–1703. doi:10.1061/(ASCE)0733-9445(2004)130:11(1692)

Shang, Y., Alipour, A., & Ye, A. (2018). Selection of input motion for seismic analysis of scoured pile-supported bridge with simplified models. *Journal of Structural Engineering*, *144*, 04018099. doi:10.1061/(ASCE)ST.1943-541X.0002067

Soneji, B. B., & Jangid, R. S. (2008). Influence of soil–structure interaction on the response of seismically isolated cable-stayed bridge. *Soil Dynamics and Earthquake Engineering*, *28*, 245–257. doi:10.1016/j.soildyn.2007.06.005

Takemiya, H., & Yamada, Y. (1981). Layered soil-pile-structure dynamic interaction. *Earthquake Engineering & Structural Dynamics*, *9*, 437–457.

Terzaghi, K. (1943). *Theoretical soil mechanics* (pp. 11–15). New York: Wiley.

Tomlinson, M.J. (1992). Foundation design and construction. London: Longman Scientific & Technical.

Touma, F. T., & Reese, L. C. (1974). Behavior of bored piles in sand. *Journal of Geotechnical and Geoenvironmental Engineering*, *100*.

Wang, Z., Dueñas-Osorio, L., & Padgett, J. E. (2014). Influence of scour effects on the seismic response of reinforced concrete bridges. *Engineering Structures*, *76*, 202–214. doi:10.1016/j.engstruct.2014.06.026

Wang, Z., Xie, X., & Wang, J. (2012). A new nonlinear method for vertical settlement prediction of a single pile and pile groups in layered soils. *Computers and Geotechnics*, *45*, 118–126. doi:10.1016/j.compgeo.2012.05.011

Wardhana, K., & Hadipriono, F. C. (2003). Analysis of recent bridge failures in the United States. *Journal of Performance of Constructed Facilities*, *17*, 144–150. doi:10.1061/(ASCE)0887-3828(2003)17:3(144)

Welch, R. C., & Reese, L. C. (1972). *Lateral load behavior of drilled shafts* (No. Interim). University of Texas at Austin.

Yang Z, Lu J, Elgamal A. (2008). OpenSees Soil Models and Solid-fluid Fully Coupled Elements, User's Manual 2008 ver 1.0. Department of Structural Engineering, UCSD, La Jolla, CA 2008

Yang, Z., Lu, J., and Elgamal, A. 2008. OpenSees soil models andsolid-fluid fully coupled elements user manual, Univ. of California,San Diego, San Diego, Calif., http://cyclic.ucsd.edu/opensees/ Jan.12, 2

Zhang, L., Zhao, M., & Zou, X. (2015). Behavior of laterally loaded piles in multilayered soils. *International Journal of Geomechanics*, *15*, 06014017. doi:10.1061/(ASCE)GM.1943-5622.0000319

Zhang, Y., DesRoches, R., & Tien, I. (2019a). Impact of corrosion on risk assessment of shear-critical and short lap-spliced bridges. *Engineering Structures*, *189*, 260–271. doi:10.1016/j.engstruct.2019.03.050

Zhang, Y., DesRoches, R., & Tien, I. (2019b). *Updating Bridge Resilience Assessment Based on Corrosion and Foundation Scour Inspection Data*. Presented at the 9th International Conference on Structural Health Monitoring of Intelligent Infrastructure (SHMII), St. Louis, MO.

Appendix

Calculating changes in soil properties due to the effect of stress history

Figures A1 and A2 show the equations and overall procedures used to obtain the updated properties of sandy (Lin et al., 2010) and clayey (Lin et al., 2014) soils, respectively, considering the effect of stress history. These procedures are incorporated in the framework of the ESHaLE model presented throughout the article.

$$\phi' = \phi'_{cs} + 3D_r\left[10 - \ln\left(\frac{P'_o}{1-\frac{2\sin(\phi')}{3-\sin(\phi')}}\right)\right] \quad \text{(a)}$$

$$\text{Before scour: } P'_o = P'_{int} = \gamma'_{int} z_{pi}\frac{3-2\sin(\phi')}{3} \quad \text{(b)}$$

$$\text{After scour: } P'_o = P'_{sc} = \gamma'_{int} z_{sc}\frac{3-2\sin(\phi')}{3} \quad \text{(c)}$$

$$OCR = \gamma'_{int} z_{pi}/(\gamma'_{sc} z_{sc}) \quad \text{(d)}$$

$$\Delta D_r = \boldsymbol{\kappa}\ln\left[\frac{(3-2\sin(\phi'))}{1+2(1-\sin(\phi'))OCR^{\sin(\phi')}}\right]/(e_{max}-e_{min}) \quad \text{(e)}$$

$$D_{r\_sc} = D_{r\_int} - \Delta D_r \quad \text{(f)}$$

$$\gamma' = \frac{(G_s-1)\gamma_w}{1+e_{max}-D_r(e_{max}-e_{min})} \quad \text{(g)}$$

$$\Delta e = -\boldsymbol{\kappa}\ln\left[\frac{1+2(1-\sin(\phi'))OCR^{\sin(\phi')}}{(3-2\sin(\phi'))OCR}\right] \quad \text{(h)}$$

ϕ' = peak effective friction angle; ϕ'_{cs} = critical effective friction angle; P'_o = initial mean effective stress; D_r = relative density; ΔD_r = change of relative density; γ' = effective unit weight; G_s = specific gravity of soil; γ_w = unit weight of water; e_{max} = maximum void ratio; e_{max} = minimum void ratio; $\boldsymbol{\kappa}$ = unloading index; K_{py} = modulus of subgrade reaction; z_{pi} = depth of point interest before scour; z_{sc} = depth of point interest after scour. Note that subscripts int and sc indicate parameters for before and after the scour event, respectively.

Determine D_{rsc} and ΔD_r iteratively based on Eqns. (d), (e), (f), (g), and (h)

↓

Determine γ'_{sc} from Eqn.(g);
ϕ'_{sc} from Eqn. (a);
OCR from Eqn. (d);
K_{py_sc} from table below

Relative density	D_r (%)	Recommended K_{py} (MN/m3)
Very loose to loose	0-35	5.4
Medium	35-65	16.3
Dense	65-100	34

Figure A1. Procedures of computing soil properties considering the effect of stress history for sandy soil.

$$\gamma'_{sc} = \frac{1+e_{int}}{1+e_{sc}}\gamma'_{int} \quad \text{(a)}$$

$$e_{int} = \frac{\gamma_w + \gamma'_{int}}{\gamma_w - \gamma'_{int} w_{int}} w_{int} \quad \text{(b)}$$

$$e_{sc} = e_{int} + C_{ur}\log\left(\frac{\sigma'_{v\_int}}{\sigma'_{v\_sc}}\right) \quad \text{(c)}$$

$$\sigma'_{v\_int} = \gamma'_{int}(z_{sc} + S_d) \quad \text{(d)}$$

$$\sigma'_{v\_sc} = (\gamma'_{sc})z_{sc} \quad \text{(e)}$$

$$\gamma'_{sc} = \frac{1+e_{int}}{1+e_{int}+C_{ur}\log\left[\frac{\gamma'_{int}(z_{sc}+S_d)}{(\gamma'_{sc})z_{sc}}\right]}\gamma'_{int} \quad \text{(f)}$$

$$\frac{C_{u\_sc}/\sigma'_{v\_sc}}{C_{u\_int}/\sigma'_{v\_int}} = OCR^{\Lambda} \quad \text{(g)}$$

$$\Lambda = \frac{\lambda - \kappa}{\lambda} = 1 - \frac{C_{ur}}{C_c} \quad \text{(h)}$$

$$OCR = \frac{\gamma'_{int}(z_{sc}+S_d)}{\gamma'_{sc} z_{sc}} \quad \text{(i)}$$

γ' = effective unit weight; e = void ratio; γ_w = unit weight of water; w = soil moisture content; C_{ur} = swelling index; C_c = compression index; C_u = soil undrained shear strength; σ'_v = vertical effective stress; z_{sc} = depth of point interest after scour; λ and κ = compression and swelling indexes from isotropic consolidation tests. Note that subscripts int and sc indicate parameters for before and after the scour event, respectively.

Determine γ'_{sc} through solving Eqn. (f)

↓

Determine σ'_{v_int} & σ'_{v_sc} from Eqns. (d) and (e);
e_{sc} from Eqn. (c);
OCR from Eqn. (i);
C_{u_sc} from Eqns. (g) and (h)

Figure A2. Procedures of computing soil properties considering the effect of stress history for clayey soil.